Lipidomic analysis of bloodstream and procyclic form *Trypanosoma brucei*

GREGORY S. RICHMOND[2]†, FEDERICA GIBELLINI[1], SIMON A. YOUNG[1], LOUISE MAJOR[1], HELEN DENTON[1], ALISON LILLEY[1] *and* TERRY K. SMITH[1]*†

[1] *Centre for Biomolecular Sciences, The North Haugh, The University, St. Andrews, KY16 9ST, Scotland, U.K.*
[2] *Present address: Agilent Technologies, Molecular Separations, Santa Clara, California 95051, USA*

(*Received 30 November 2009; revised 13 March, 21 and 22 April 2010; accepted 22 April 2010*)

SUMMARY

The biological membranes of *Trypanosoma brucei* contain a complex array of phospholipids that are synthesized *de novo* from precursors obtained either directly from the host, or as catabolised endocytosed lipids. This paper describes the use of nanoflow electrospray tandem mass spectrometry and high resolution mass spectrometry in both positive and negative ion modes, allowing the identification of ~500 individual molecular phospholipids species from total lipid extracts of cultured bloodstream and procyclic form *T. brucei*. Various molecular species of all of the major subclasses of glycerophospholipids were identified including phosphatidylcholine, phosphatidylethanolamine, phosphatidylserine, and phosphatidylinositol as well as phosphatidic acid, phosphatidylglycerol and cardolipin, and the sphingolipids sphingomyelin, inositol phosphoceramide and ethanolamine phosphoceramide. The lipidomic data obtained in this study will aid future biochemical phenotyping of either genetically or chemically manipulated commonly used bloodstream and procyclic strains of *Trypanosoma brucei*. Hopefully this will allow a greater understanding of the bizarre world of lipids in this important human pathogen.

Key words: Phospholipid, *Trypanosoma brucei*, mass spectrometry, lipidomics.

INTRODUCTION

Phospholipids (PLs) are vital and ubiquitous components of the cell membrane bilayer that delineates the confines of a cell and its subcellular compartments. The major classes of glycerophospholipids include: phosphatidic acid (PA), phosphatidylglycerol (PG), phosphatidylinositol (PI), cardiolipin (CL) and the aminoglycerophospholipids: phosphatidylcholine (PC), phosphatidylethanolamine (PE) and phosphatidylserine (PS) (Fahy *et al*. 2005). Considering that their hydrophobic chains can vary in length and degree of unsaturation, a wide variety of different molecular species of each phospholipid class are possible. This diversity allows the formation of highly specialised membranes with unique functions; also the alteration of the membrane lipid composition allows the cell to respond to environmental changes. The glycerophospholipid composition of membranes varies with cell type in multicellular organisms, and is different in the individual organelles in eukaryotic cells. The composition also depends on growth conditions, such as pH, temperature and the growth phase; lipids are also not equally distributed across the two leaflets of a membrane bilayer (Zachowski, 1993). Furthermore, in higher eukaryotes bioactive precursors stored in PLs and released by phospholipases have been recognized as important factors in signal transduction and in the generation of lipid mediators, such as eicosanoids (James and Downes, 1997; Six and Dennis, 2000). Phospholipase-modified PLs are themselves important mediators in cellular processes such as apoptosis and membrane trafficking (Fadok *et al*. 2001; Ishii *et al*. 2004).

Trypanosoma brucei, the causative agent of African sleeping sickness, belongs to the order Kinetoplastida, which are considered part of the earliest diverging eukaryotic lineages (Michels *et al*. 2000). As such, there is an historical precedence to regard *T. brucei* as a 'model organism' for the study of alternative mechanisms by which eukaryotes accomplish basic functions (Michels *et al*. 2000). During their life-cycle they encounter vastly different environments and respond to these by dramatic morphological and metabolic changes, including adaptation of their lipid and energy metabolism (Michels *et al*. 2000). Lipids constitute 11–18% of the dry weight of *T. brucei* and their distribution is consistent with the usual range of lipids found in eukaryotes, such as phospholipids, neutral lipids, sterols, fatty acids, plasmalogens, isoprenoids and sterols (Dixon and Williamson, 1970; Dixon *et al*. 1971; Venkatesan and Ormerod, 1976; Patnaik *et al*. 1993; Smith, 1993; Vial *et al*. 2003).

T. brucei contains all the major phospholipid classes, accounting for ~80% of membrane lipids

* Corresponding author: Tel: (0)1334-463412; E-mail: tks1@st-andrews.ac.uk

† These authors contributed equally.

doi:10.1017/S0031182010000715

(Patnaik *et al*. 1993). Trypanosomes do not utilise the intact phospholipids they scavenge from their hosts, but use their repertoire of metabolic and anabolic enzymes to synthesise their own phospholipids and glycolipids *de novo* as per their specific requirements (Dixon and Williamson, 1970; van Hellemond and Tielens, 2006). Until relatively recently most of the literature on *T. brucei* lipid metabolism involved myristate metabolism and its requirement for glycosylphosphatidylinositol (GPI) anchor biosynthesis (Buxbaum *et al*. 1994, 1996). With the completion of the *T. brucei* genome, several biosynthetic enzymes involved in *de novo* synthesis of phospholipids have been studied, including: sphingomyelin synthases, a phospholipase A1, the phosphatidylinositol synthase and enzymes of the Kennedy pathway involved in *de novo* PE and PC synthesis – this has been reviewed recently (Smith and Bütikofer, 2010).

Since many pathogens have developed unique membrane structures and specialised lipid biosynthetic pathways that differ from those of the host, the study of lipid metabolism could unravel novel drug targets for therapeutic intervention. As progress in research elucidates lipid metabolism in greater detail in parasites and hosts, and more enzymes involved in phospholipid metabolism are characterized, new targets are likely to emerge for the development of new anti-protozoan drugs. For example, it has been shown that a possible mechanism of action of the lysophospholipid analogues, miltefosine, edelfosine and ilmofosine, against *Leishmania* and *Trypanosoma cruzi* proceeds through the inhibition of PC biosynthesis (Urbina, 2006). Bisthiazolium compounds are choline analogues showing strong potency against the malaria parasite *Plasmodium falciparum* and they were shown to target PC biosynthesis from choline and ethanolamine (Le Roch *et al*. 2008).

In trypanosomes, as with other cells, older methods of PL analysis relied heavily upon thin layer chromatography to separate and identify various PL classes. Subsequently gas chromatography was employed to analyze the overall fatty acid composition (Godfrey, 1967; Dixon and Williamson, 1970). Later some *T. brucei* PL molecular species were identified by benzoyl derivatisation of the diradylglycerols derivatives followed by thin layer chromatography separation of diacyl, alkylacyl and alkenylacyl fractions prior to reverse phase chromatography/mass spectrometry (Patnaik *et al*. 1993). These older methods are time, labour and material expensive, which makes these multi-step analyses vulnerable to oxidation and other modifications during preparation. Although not used to study *T. brucei* lipid composition, fast atom bombardment MS has alleviated many of these disadvantages and allowed sensitive analysis of intact lipids (Chilton and Murphy, 1986). The next generation of MS technology, electrospray ionization tandem mass spectrometry (ESI-MS-MS), allows 'soft' ionization of biomolecules without chromatographic separation or derivatization, and has the benefit of high sensitivity and reproducibility (Kerwin *et al*. 1994; Brugger *et al*. 1997). ESI-MS-MS allows specific detection of the major PL classes and subclasses, and their molecular species, from the same sample. This methodology has proved an efficient tool for examining alterations in the cell's lipidome after cellular perturbations, either genetically or chemically. For instance, it has been used to analyze global changes in the PL content of sphingomyelin-deficient and alkylacyl/alkenylacyl PL-deficient *Leishmania major* (Zufferey *et al*. 2003; Denny *et al*. 2004), and knock-outs or knock-downs of enzymes involved directly or indirectly in *de novo* lipid synthesis in *T. brucei* (Voncken *et al*. 2003; Martin and Smith 2006*a*, *b*; Richmond and Smith 2007*a*, *b*; Güler *et al*. 2008; Signorell *et al*. 2008; Gibellini *et al*. 2009 and reviewed in van Hellemond and Tielens, 2006).

Here we report the lipidomes of commonly used laboratory strains BSF and PCF *T. brucei*, characterizing ~500 individual molecular phospholipid species. This will provide a useful tool to the community to aid future biochemical phenotyping of either genetically or chemically altered *T. brucei*.

MATERIALS AND METHODS

Materials

All solvents were analytical HPLC grade and from BDH. Glassware was used at all times after the introduction of solvent to the samples, except when loading samples into nanoflow tips. Glassware was solvent washed and positive displacement pipettes with glass tips were used to measure solvent quantities, where possible. Ethanol-1,1,2,2-d4-amine (d_4-ethanolamine) were from CDN Isotopes. The non-natural phospholipid standards 1,2-diheptadecanoyl-*sn*-glycero-3-phosphate, PA (17:0/17:0); 1,2- dipentadecanoyl-*sn*-glycerol-3-phosphoethanolamine PE (15:0/15:0); 1,2-dimyristoyl-*sn*-glycero-3-[phospho-rac-(1-glycerol)], PG (14:0/14:0); 1,2-diheneicosanoyl-*sn*-glycero-3-phosphocholine, PC (21:0/21:0); 1,2-dimyristoyl-*sn*-glycerol-3-[phospho-L-serine], PS (14:0/14:0); 1-dodecanoyl-2-tridecanoyl-*sn*-glycero-3-phospho-(1′-*myo*-inositol), PI (12:0/13:0); and 1,2 dipalmitoyl-*sn*-glycerol, DAG (16:0/16:0), were purchased from Avanti Polar Lipids.

T. brucei *cell culture*

Bloodstream form (BSF) trypanosome cultures (strain 427, MITat 1.2) were maintained in HMI-9 media at pH 7·5, supplemented with 10% heat-inactivated foetal calf serum (PAA Labs) and 10% Serum Plus (JRH Biosciences). Cells were grown in Cell star tissue culture flasks with air filter lids

(Greiner) and incubated in a humidified 37 °C incubator with 5% CO_2. The BSF *in vitro* culture cell line used throughout this study is from the long-term cultures of 'single marker' cells that express a tetracycline repressor and T7 RNA Polymerase (Wirtz *et al*. 1999). This transgenic parental cell line was maintained under neomycin (G418) drug pressure at a final concentration of 2·5 μg/ml. Cultures were normally maintained below a cell density of 2×10^6/ml before lipid extraction. Procyclic form (PCF) trypanosome cultures were maintained in supplemented SDM-79 media at pH 7·4 which contained 15% heat-inactivated foetal calf serum as a lipid source, 2 g/L $NaHCO_3$, 2·5 mg/ml haemin and 1x Glutamax (Invitrogen). Cells were grown in non-tissue culture treated flasks (Falcon) in a humidified 28 °C incubator with 5% CO_2. The PCF *in vitro* culture cell line used throughout these studies is from the long-term cultures of 'double marker' cells that express a tetracycline repressor and T7 RNA polymerase. This transgenic parental cell line was maintained under neomycin (G418) and hygromycin drug pressure at final concentrations of 15 μg/ml and 50 μg/ml, respectively. Cultures were normally maintained below a cell density of 2×10^7/ml before lipid extraction.

Lipid extraction

Lipids were extracted according to the method of Bligh and Dyer (Bligh and Dyer, 1959). To detect minor mass constituents a relatively high concentration of cells was used; when better resolution between individual molecular species peaks was desired, the sample was diluted with more solvent. Normally, 10^8 cells were harvested, washed twice in TDB, (25 mM KCl, 400 mM NaCl, 5 mM $MgSO_4$, 100 mM Na_2HPO_4, NaH_2PO_4, 100 mM glucose) and resuspended in 100 μl TDB in a glass vial prior to lipid extraction. A mixture of the internal standards (50 pmoles of each, except PI which was 20 pmoles) was added prior to removal of the lower cholorform rich phase. This allowed normalization of the data obtained from the high-resolution mass spectra and to ensure correct fragmentation of individual phospholipids species.

The lipid-rich lower phase was washed by mixing it with 225 μl of upper phase from a blank sample. The resultant lower phase was transferred to a new vial and dried under nitrogen. The lipids were resuspended with chloroform/methanol (1:2 v/v) to the desired volume (10–40 μl), just prior to ESI-MS-MS analysis. The vials were centrifuged at 5000 × *g* for 1 min. Samples were usually processed and analyzed the same day, but if short-term storage was necessary the lipids were stored dried under a nitrogen atmosphere at 4 °C.

High-resolution mass spectrometry

An aliquot of the total lipid extract was analyzed with both an electrospray ionisation mass spectrometer (LCT, Micromass) and a QStar mass spectrometer (Applied Biosystems) both equipped with nanoelectrospray sources. Samples were loaded into thin-wall nanoflow capillary tips (Waters) and analyzed in both positive and negative ion mode.

Each spectrum encompasses at least 50 repetitive scans (400–2000 m/z). Spectra were processed using Micromass software; a high-resolution peak list was generated and normalized to the masses of the non-natural internal standards. Isotope ions were eliminated, i.e. due to naturally occurring ^{13}C (1·1%). The resulting high-resolution data were normalized using the internal standards. These data have been annotated to the corresponding phospholipid species in Supplementary Tables 1–8 (see Appendix), the accurate masses correspond to the mean (± 0·05 m/z) of 4 separate determinations using the two different instruments.

Nano-electrospray ionization tandem mass spectrometry (nano-ESI-MS-MS)

An aliquot of total lipid extract was analyzed with a Micromass Quattro Ultima triple quadrupole mass spectrometer equipped with a nanoelectrospray source. Samples were loaded into thin-wall nanoflow capillary tips (Waters) and analyzed by ESI-MS-MS in both positive (for phosphatidylcholine (PC), sphingomyelin (SM), phosphatidylserine (PS) and phosphatidylethanolamine (PE)), and negative ion mode (for PI, phosphatidylglycerol (PG), phosphatidic acid (PA), PS and PE). Capillary/cone voltages were 0·7 kV/50 V and 0·9 kV/50 V for positive ion and negative ion modes, respectively. Tandem mass spectra (MS-MS) were obtained using argon as the collision gas (~3·0 mTorr) with collision offset energies as follows: 35 V, PC in positive ion mode; 25 V, PE in positive ion mode; 22 V, PS in positive ion mode; 50 V, PE in negative ion mode; 28 V, PS in negative ion mode; 45 V, PI in negative ion mode; and 50 V, all glycerophospholipids detected by precursor scanning for *m/z* 153 in negative ion mode. MS-MS daughter ion scanning was performed with a collision-offset energy of 35 V. In positive ion mode, ions in the PC, PE, and PS spectra were annotated based on their $[M+H\text{-}NMe_3]^+$ for PC, and the corresponding fragment ions [M-140] and [PA-H] daughter ions for PE and PS respectively, and compared with that of their theoretical values. In negative ion mode, PL class peaks were assigned according to their $[lyso\text{-}H]^-$, $[lyso\text{-}H_20\text{-}H]^-$, $[lysoPA\text{-}H]^-$, or $[lysoPA\text{-}H_20\text{-}H]^-$ daughter ion derivatives. FAs were assigned based on their $[M-H]^-$ values. Saturated and unsaturated FAs were assumed to be esterified to the *sn*-1 and *sn*-2 position of PLs,

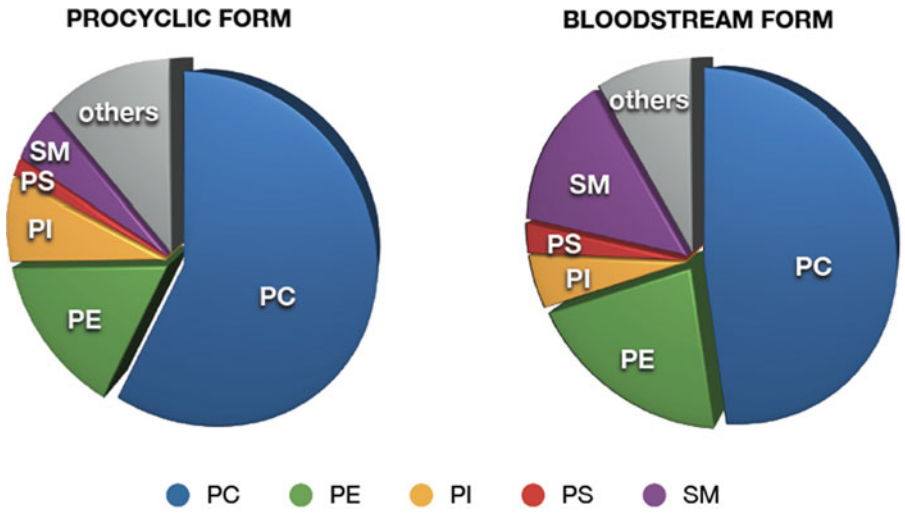

Fig. 1. Phospholipid composition of PCF and BSF *T. brucei*. PC, phosphatidylcholine; PE, phosphatidylethanolamine; PI, phosphatidylinositol; PS, phosphatidylserine; SM, sphingomyelin. "Others" include: inositol phosphoceramide, phosphatidic acid, phosphatidylglycerol, cardiolipin, PIPs, lyso-PC and lyso-PE.

respectively. Each spectrum (600–1000 m/z) encompasses at least 50 repetitive scans, each of 4 s duration. Spectra were normally processed by subtraction of background and smoothed using Micronass processing algorithms unless otherwise indicated. The internal standards were used to ensure efficient ionization and fragmentation and as a control for sample variability.

Stable isotope labeling of bloodstream form T. brucei

$2{\cdot}5\times10^7$ *T. brucei* bloodstream-form cells at a density of $0{\cdot}5\times10^6$ cells/ml were incubated overnight at 37 °C in HMI-9 media supplemented with 1 mM d_4-Etn. Total lipids were extracted and processed using a nano-ESI-MS-MS as described earlier. $[M-H]^-$ adducts of unlabelled PE and (d_4)-labelled PE were monitored by parent ion scanning for m/z 196 and 200, respectively. $[M+H]^+$ adducts of unlabelled PC and (d_4)-labelled PC were monitored by parent ion scanning for m/z 184 and 188, respectively.

RESULTS AND DISCUSSION

Phospholipid composition

Quantification of the phospholipids in bloodstream and procyclic *T. brucei* shows the most abundant glycerophospholipid classes are PC and PE representing 45–60% and 10–20%, while PI, PS, PG and CL represent minor glycerophospholipid classes (Fig. 1). These values compare well with previous quantifications of phospholipids in *T. brucei* (Patnaik *et al*. 1993). *T. brucei* also contain sphingolipids, such as sphingomyelin (SM), inositol phosphorylceramide (IPC) and ethanolamine phosphorylceramide (10–15% in total).

High-resolution mass spectra were collected both in positive and negative ion mode for BSF and PCF *T.brucei* total lipid extracts (Figs 2 and Fig. 3, respectively). In the positive ion mode, ions represents $[M+H]^+$ and $[M+Na]^+$ of PC, SM and to a minor extent PE and PS species, while in the negative ion mode, ions represent $[M-H]^-$ of PI, PE, PS, PG and PA species. Peak lists from these data were normalized using the added non-natural internal standards. After averaging, these data were used to clarify some of the phospholipid identities given in Tables S1–S8 (see Appendix). ESI-MS-MS was also employed to separate and characterize the major PL classes and their molecular species from total lipid extracts of *T. brucei*. Together these two sets of data allow the identity of ~500 individual molecular phospholipid species to be determined.

Fatty acid composition of PL

Analysis of the acyl content of the various phospholipids suggests that the intrinsic acyl-CoA specificity of the acyltransferases involved in diacyl and ether-linked phospholipid *de novo* synthesis and the availability of *de novo* synthesised acyl-CoAs are major factors in producing the final molecular composition of the phospholipids species. The major ether-linked PE and PC species and the diacyl linked PC, PE, PI and PS species contain almost exclusively *sn*-1 C18:0. This implies both the acyltransferases that service dihydroxyacetone-phosphate and glycerol-3-phosphate have either a specificity for C18:0-CoA or are exposed exclusively to C18:0-CoA. The *sn*-2 position of these lipid species are almost exclusively unsaturated acyl groups, with ether-linked lipids

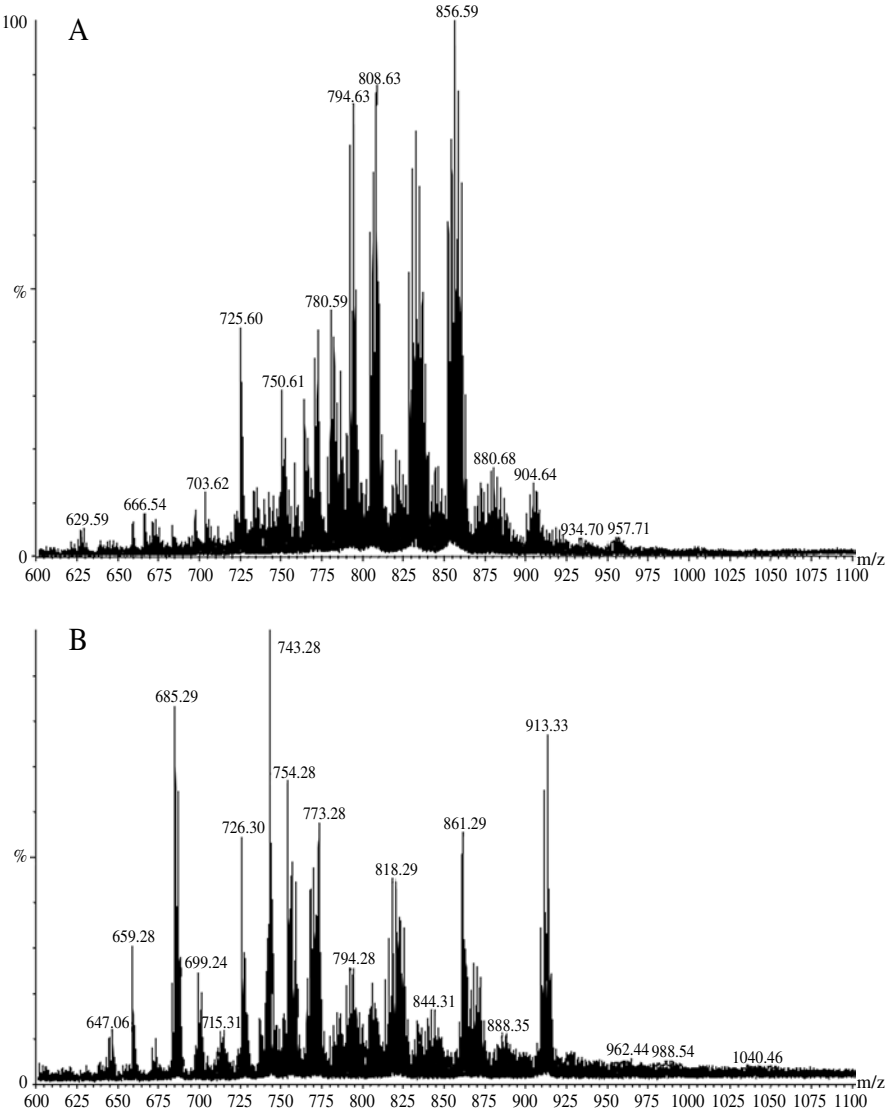

Fig. 2. High resolution survey scans in positive (A) and negative (B) ion mode of total lipid extracts from BSF *T. brucei*.

containing predominately C18:2, while diacyl lipids contain mainly C18:2 and C22:4, with minor C20:4.

In *T. brucei* procyclic forms, the relative amounts of diacyl glycerophospholipids containing highly unsaturated fatty acyl chains showed a decrease compared to bloodstream forms, in the order of PC > PE > > PI. *T. brucei* parasites also contain significant proportions of *sn*-1 ether-linked glycerophospholipids, especially in PE (73–84%) and PS (60–88%).

Choline PL composition

In positive ion mode, $[M+H]^+$ ions of PC and SM are detected by colliding ions with argon to create various fragment ions and, in the case of choline-containing PLs like PC and SM, an intense *m/z* 184 fragment is produced. Thus, a positive ion precursor scan for *m/z* 184 detects all PC and SM $[M+H]^+$ ions and their natural isotopes, each represented as a *m/z* signal in a spectrum. Colliding ions from the mono-isotopic signals produces specific daughter ion fragments which are used to correctly assign the *m/z* signal to a molecular species that contains a certain number of FA carbons and which have an associated degree of unsaturation. In positive ion mode, individual FAs cannot be discerned and thus the FA moiety is represented as a sum of FAs in the form x:y, where 'x' is the total number of FA carbons and 'y' is total number of double bonds in both FA chains. As portrayed in this report, a peak in the spectrum consists of a series of molecular species of a particular class of PL with the same number of carbon atoms, but with different masses due to heterogeneity in their state of unsaturation.

The pool of PC and SM lipids in both PCF and BSF lipid extracts of *T. brucei* is comprised of numerous molecular species (Fig. S1 A and B, respectively, see Appendix). Annotation of these

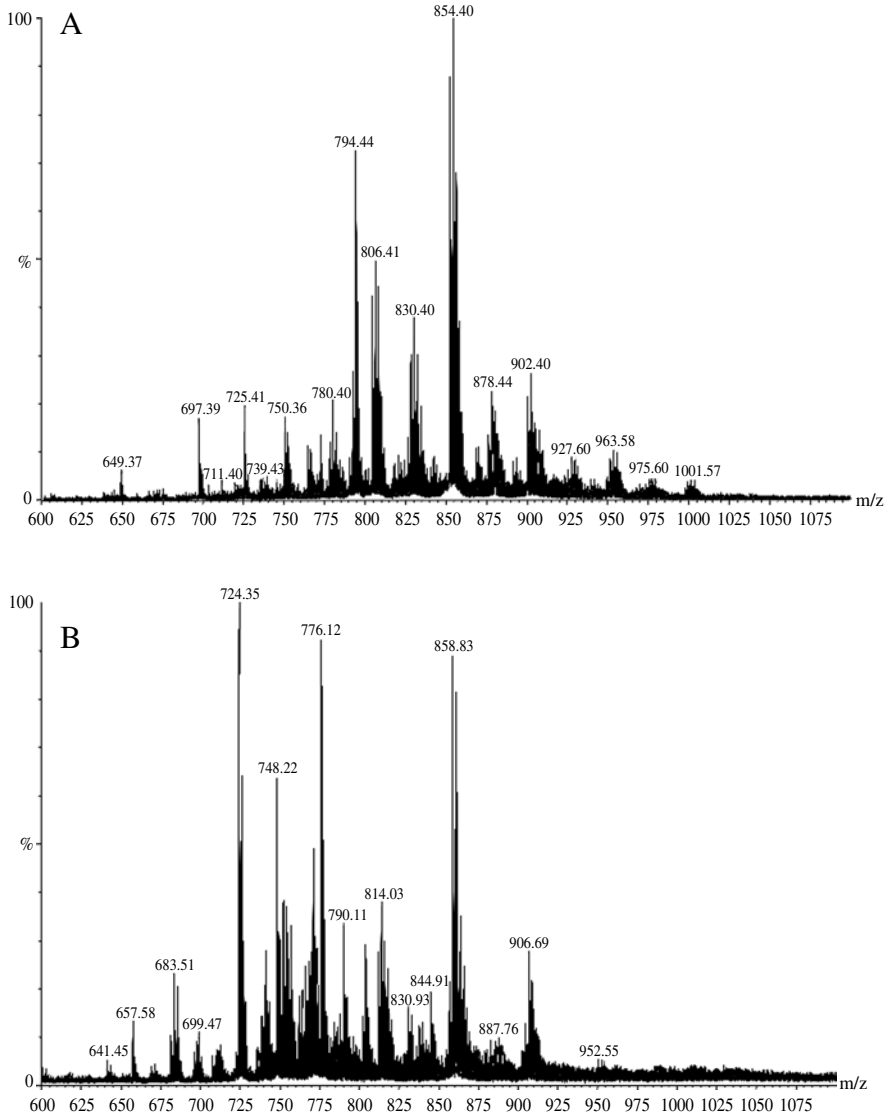

Fig. 3. High resolution survey scans in positive (A) and negative (B) ion mode of total lipid extracts from PCF *T. brucei*.

species is provided in Tables S1 and S2, respectively. Analysis of the ions in the spectra (Fig. 4) revealed that the *T. brucei* PC pool contains molecular species from both the diacyl and ether PL subclasses. The ratio between diacyl and ether PC in both PCF and BSF cells was roughly 3:1. These subclasses of phospholipids in *T. brucei*, as with other eukaryotes, are defined by their *sn*-1 fatty acyl bond and are referred to as either one of the following types: (1) diacyl; (2) plasmanyl (a, alkylacyl); or (3) plasmenyl/plasmalogen (e.g. alkenylacyl). It is important to note that, in both life cycle stages, for nearly every diacyl PC series there appears to be an alkylacyl/alkenylacyl PC counterpart. These results contrast with those from a previous study, which reported that the only ether-linked PC species in BSF *T. brucei* was PC (e/a-36:2 – reported as e/a-18:0/18:2, Patnaik *et al.* 1993). PC (e/a-18:/18:2) is indeed the most abundant ether PC in BSF trypanosomes, but heterogeneity does exist since e/a-PC with other FA chain lengths were detected. A drawback to identifying PLs by ESI-MS-MS is that it is not possible to differentiate between alkyl and alkenyl *sn*-1 linkages in many instances without their prior chromatographic separation. For instance, an ether-linked a-18:1 and a vinyl ether-linked e-18:0 possess equivalent masses. For the *m/z* 822 PC species in Table S1 (see Appendix), for example, the presence of *sn*-2 22:4 with ether-linked e/a-18:y could therefore indicate the existence of two species with identical masses, PC (a-18:1/22:4) and/or PC (e-18:0/22:4).

Relative molar composition of PC molecular species was calculated by integrating the relative area of the peaks of each series. Such percent composition analysis showed that, in BSF trypanosomes for instance, the four main series in the PC spectrum comprised 34·4%, 19·1%, 13·6%, and 13·0% of total PC in the cell, and they originated from signals in the 40:y, 36:y, 38:y, and e/a-36:y series, respectively (Fig. 4, Table S2, Appendix). The major peak areas from these series are mostly comprised of the following species of PC: *m/z* 834, 40:6; *m/z* 836,

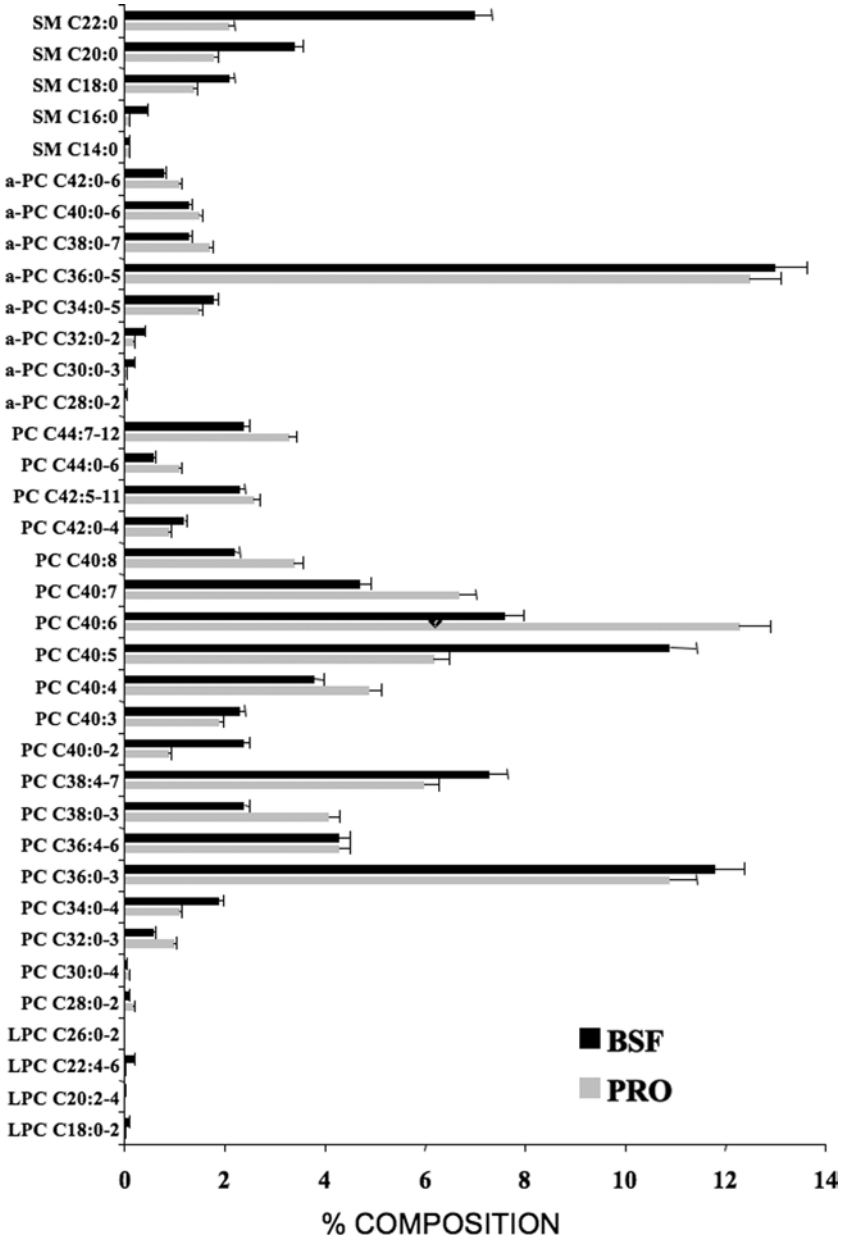

Fig. 4. Molecular composition of choline-containing PLs in *T. brucei*. Precursor ion scanning for *m/z* 184 specifically detected $[M+H]^+$ PC and SM ions from PCF and BSF trypanosome total lipid extracts see Figs. S1 and S2. Molecular species are plotted against their relative percentage based upon TIC, PCF (BLACK) and BSF (GREY). Peak assignments are based on MS-MS daughter ion spectra performed as stated in the Material and Methods, and each peak is annotated in Tables S1 and S2.

40:5; *m/z* 838, 40:4; *m/z* 786, 36:2; *m/z* 788, 36:1; *m/z* 790, 36:0; *m/z* 810, 38:4; *m/z* 812, 38:3; *m/z* 814, 38:2; *m/z* 774, a-36:1 and/or e-36:0; *m/z* 772, a-36:2 and/or e-36:1. Analysis of the spectra also revealed that *T. brucei* possesses PC (42:y) and PC (44:y), unusual species that most likely contain long-chain poly-unsaturated FAs (PUFAs) and highly unsaturated FAs (HUFAs) at the both the *sn*-1 and *sn*-2 positions (Fig. S4, peaks N and O). The most abundant PUFAs and HUFAs in *T. brucei*, whose combinations could mostly satisfy the FA requirements in PC (42:y) and PC (44:y), are 22:4, 22:5, 22:6, 20:2, 20:3, 20:4, and 20:5 (Fig. 4). It is also possible that the FA 24:1 may be a constituent of these species as this FA has been reported to exist in PLs of *T. brucei* [20]. PC (42:y) and PC (44:y) have not been detected before in *T. brucei* but they have been noted in another kinetoplastid, *Leishmania major* (Zufferey *et al*. 2003; Denny *et al*. 2004).

Comparisons of the PC profile from PCF and BSF total lipid extracts (Fig. 4) showed that there were minor alterations in the prominence of FA unsaturation states in some series. For instance, analysis from a multitude of runs (>8) showed that the PC (40:6) signal in PCF cells was consistently more intense than the PC (40:5) signal, whereas in BSF

cells the situation is reversed (see Figs 4, S4A and B, and compare Tables S1 and S2, Appendix). A similar pattern was observed for the PC (44:n) species.

It is noteworthy that the relative amounts of SM in PCF cells is significantly lower compared to the SM levels in BSF cells (Figs 1 and 4). This is observed by comparing peaks C, E, and G in the BSF and PCF spectra (Figs S4A and B, respectively Appendix). This is due in part to the ceramide which is normally used in conjunction with PC to form SM, by the sphingomyelin synthases, is now also being used to form inositol phosphoceramide (IPC) from PI in PCF trypanosomes (Fridburg *et al*. 2008; Sutterwala *et al*. 2008).

Another PL component in *T. brucei* membranes is lyso-PC, which is synthesized from the action of a novel phospholipase A_1 in this organism (Richmond and Smith, 2007*a*, *b*). Detection of lyso-PC was achieved only after restricting the scanned mass range in the 184 m/*z* precursor ion scans to exclude the mass range in which the major PC ions fall (Fig. S2). Analysis of the lyso-PC spectra revealed distinct lyso-PC species (Fig. 4); the most abundant species contain one of the following *sn*-2 FA constituents: 18:0, 18:1, 18:2, 20:2, 20:3, 20:4, 22:4, 22:5 and 22:6. The levels of lyso-PC are higher in BSF than in PCF trypanosomes. Also, PCF cells appeared to contain more lyso-PC (-/22:6), whereas the major BSF lyso-PC species was (-/22:5).

PE composition

In negative ion mode, ions of PI, PA, PG, PS and PE species are efficiently detected. Collision-induced dissociation of PLs containing an ethanolamine-phosphate head group produces a unique fragment ion of *m*/*z* 196, and precursor scanning for this ion from total lipids extracted from PCF and BSF cells selectively detected $[M-H]^-$ ions of PE (Figs S6A and B, annotated species in Tables S3 and S4, respectively). The striking feature about this class of phospholipid is the dominating presence of the ether PE series e/a-36:y (Fig. 5). The principal signal within this series specifically represents the *m*/*z* 726 $[M-H^-$ ion (Figs S6A and B, Appendix). From daughter ion scanning the species was deduced to be PE (e-18:1/18:2) instead of either PE (a-18:0/18:3) or PE (a-18:1/18:2); this result is consistent with the previous finding that there is 2–4 times as much alkenylacyl PE than alkylacyl PE in *T. brucei* (Patnaik *et al*. 1993). As with PC, it was originally reported that 100% of all the alkylacyl and alkenylacyl PE in BSF *T. brucei* was from just one molecular species, PE (e/a-18:0/18:2), which is certainly by far the major species. However, daughter ion scanning of the PE spectra ions from the ESI-MS-MS method revealed multiple ether lipid species in both the PCF and BSF parasite stages (Fig. 5 and annotated in Tables S3 and S4 respectively).

The relative abundance of diacyl PE in BSF cells is slightly higher than in PCF cells (36% vs. 19%, respectively). This is most likely due to the increased availability of host PUFA resulting in PE species with longer acyl chains, particularly the 40:y and 42:y series (Fig. 5).

PE can also be detected in positive ion mode by scanning for the neutral loss of *m*/*z* 141. However, the results from negative mode give more accurate reflections of the true abundances of ether PE series (Brugger *et al*. 1997). This is also true for *T. brucei* where ether PE species in PCF and BSF parasites make up 81% and 64% of total PE in the cell, respectively; these values correlate well with those obtained previously (Patnaik *et al*. 1993). However, in positive ion mode, the *m*/*z* 141 neutral loss scans show the combined relative abundances of all the diacyl species (>87%) far exceeded that of all the ether lipid species (data not shown), thus giving an inaccurate reflection of the true PE status of a *T. brucei* cell, and confirming that analyzing PE in negative ion mode is preferable.

PE cannot be converted into PC in T. brucei

PC and PE are the two major phospholipid classes in eukaryotic cells and their metabolism is highly interconnected. They are both synthesised *de novo* through branches of the Kennedy pathway (Kennedy and Weiss, 1956; Kanfer and Kennedy, 1963; recently reviewed in Gibellini and Smith, 2010). PE can also be converted into PC by three subsequent SAM dependent methylations of the ethanolamine headgroup. However, in *T. brucei* the methyltransferase genes could not be found (http://www.tritrypdb.org). This surprising absence of PE methylation was experimentally confirmed by stable isotope labelling of bloodstream-form *T. brucei* with the PE precursor d4-ethanolamine followed by analysis of PE and PC molecular species by ESI-MS/MS (Fig. 6).

PE and PC that incorporate the deuterium-labelled ethanolamine can be easily distinguished from their non-labelled counterparts because they produce fragments at higher m/z: 200 m/z for the deuterated ethanolamine-phosphate-glycerol-H_2O instead of 196 m/z and 188 m/z for the deuterated phosphocholine instead of 184 m/z in positive ion mode (Figs 6 A–D respectively).

The d_4-ethanolamine is readily taken up by the parasite by an as yet unknown transporter, and incorporated into d_4-PE, and its molecular species profile is virtually super-imposable with the one of the unlabelled PE (Fig. 6A and B). However, the complete absence of d_4-PC species (Fig. 6D), demonstrates that there is no conversion of d_4-PE to d_4-PC. The spectrum including the cellular species of PC is shown in Fig. 6C as a comparison. This indicates that there is no methylation of PE under these

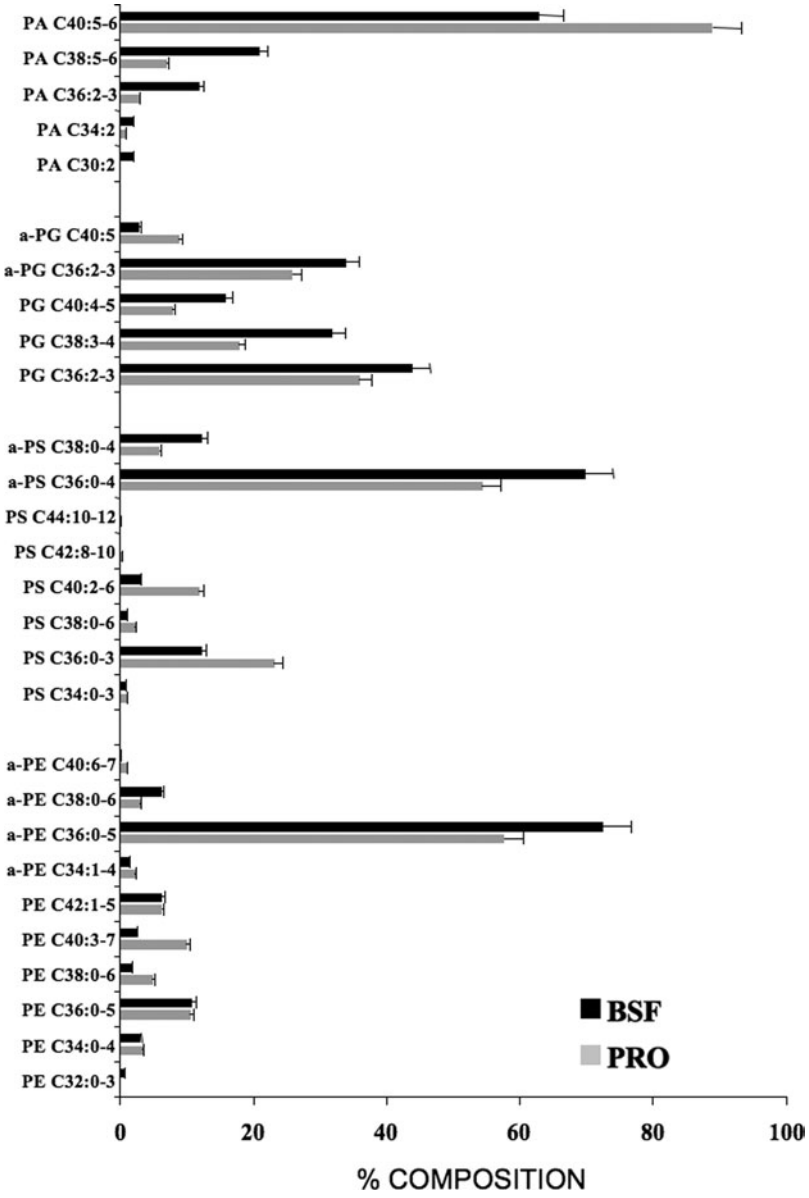

Fig. 5. Molecular composition of PE, PS, PA and PG species in *T. brucei*. Precursor ion scanning for *m/z* 196 specifically detected $[M-H]^-$ PE ions from PCF and trypanosome total lipid extracts see Fig. S3. Molecular species are plotted against their relative percentage based upon TIC, PCF (BLACK) and BSF (GREY). Peak assignments are based on MS-MS daughter ion spectra performed as stated in the Material and Methods section, and a letter annotates each peak series, which are annotated in Tables S3–S6.

conditions, thus all *T. brucei* choline is scavenged from its host, and thus they are auxotropic for choline. Given the fact that they can not take up choline, as they do not process a choline transporter (experimentally verified with radio- and stable-isotope labelled choline, T. K. Smith, unpublished observations), suggests that all *T. brucei* choline comes from endocytosed choline containing phospholipids such as PC, lyso-PC and SM, some of which (probably a large proportion) will be endocytosed as low density lipoprotein particles (Overath and Engstler, 2004).

A search in the genomic database for trypanosomatid pathogens, the Tri-TrypDB (http://tritrypdb.org/), revealed that the PE N-methyltransferase genes are also absent in *T. cruzi*, but are present in *Leishmaina* species; their presence has been experimentally confirmed in *Leishmania major* (T. K. Smith, unpublished observation), while in *Plasmodium falciparum* they have plant-like N-methyltransferase genes (Pessi *et al*. 2005).

PS composition

The molecular composition of PS species in *T. brucei* has not been determined before, but it accounts for ~3% of the total PL in *T. brucei*. Scanning for a neutral loss of *m/z* 87 from collision-induced dissociation of ions in negative mode specifically identifies PS molecules (Figs S4 A and B, Appendix). The

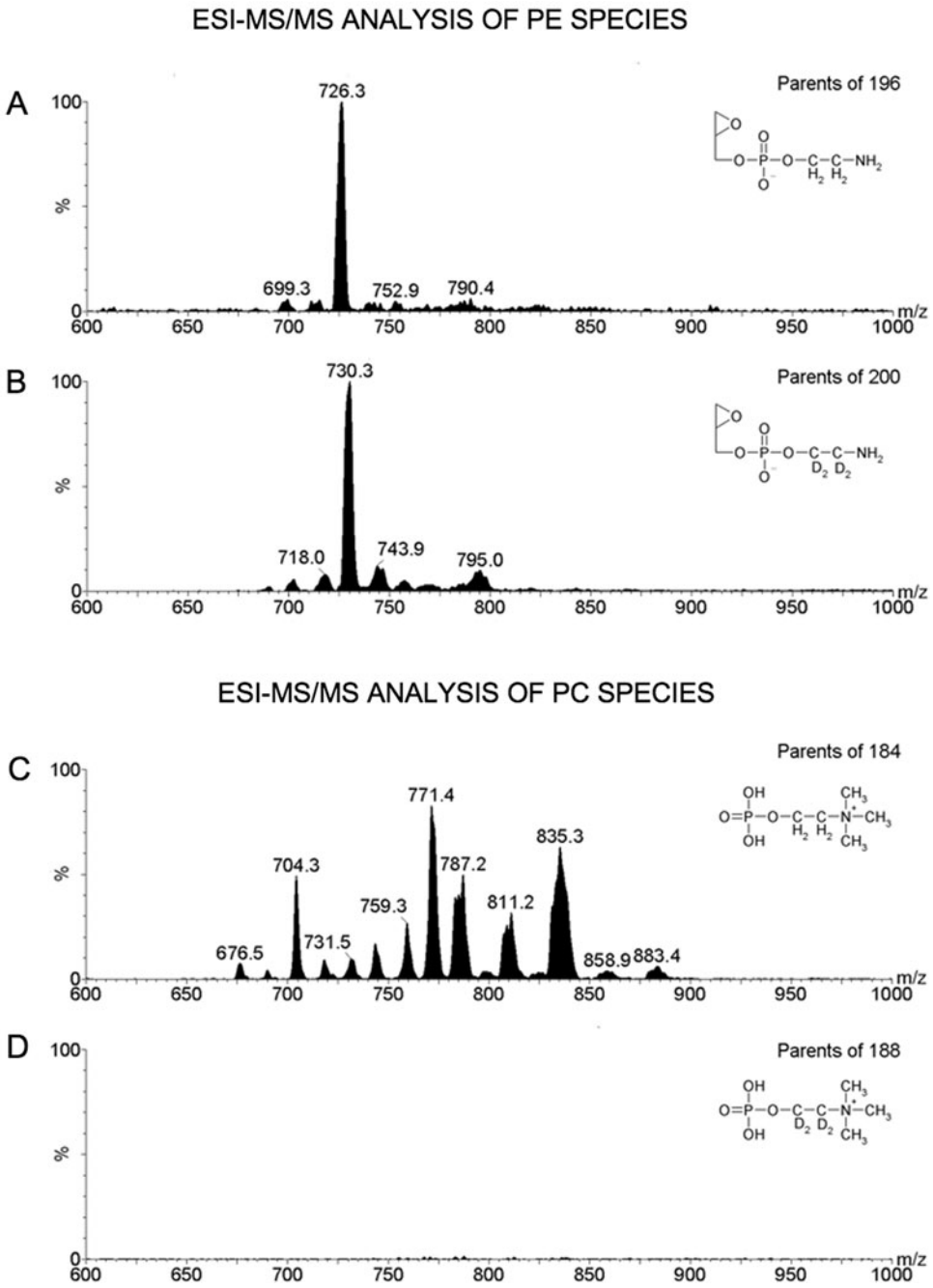

Fig. 6. *T. brucei* have no N-methyltransferases capable of converting PE to PC. ESI-MS/MS spectra of the following molecular species; PE (A); (d4)-PE (B); PC (C); (d4)-PC (D), in BSF *T. brucei* labelled with (d4)-ethanolamine. Data were normalised to the largest peak and vertical axes linked in order to directly compare the intensities of non-deuterated vs. deuterated phospholipid species. Also shown are the molecular structures of the relevant collision-induced fragments.

PS pool in PCF and BSF *T. brucei* contains a variety of diacyl and ether molecular species (Tables S5 and S6 respectively, see Appendix), the latter of which is 60–77% in the alkylacyl subclass (Fig. 5). The most intense signal stems from m/z 772 (Figs. S4 A and B), which represents the $[M-H]^-$ ion of PS (a-18:0/18:2) . Nearly a quarter ($\sim$24%) of all PS species are of the diacyl series 36:y in BSF trypanosomes but this level is decreased to $\sim$12% in PCF cells (Fig. 5), along with a significant decrease in the amount of series 40:y, probably due to a lack of host PUFA as discussed for the PE species. These two observed differences probably account for most of the increase in diacyl PS in BSF compared to PCF trypanosomes (Patnaik *et al*. 1993).

PS can also be detected in positive ion mode by scanning for the neutral loss of m/z 185. Performing this scan from total lipids in BSF and PCF parasites revealed more molecular species of PS than did the m/z 87 neutral loss scan (data not shown). However, as

with the alternative PE scan, the intensities of the diacyl and ether PE signals did not match the known abundances of those subclasses. Ether PS makes up 81–88% and 61% of all PS in PCF and BSF cells, respectively (Fig. 5), but the neutral loss *m/z* 185 scan in the BSF, for example, only showed a cumulative ether PS content of approximately 10% of total PS (data not shown).

PE cannot be formed by decarboxylation of PS in BSF T. brucei

A possible alternative route to the Kennedy pathway for the biosynthesis of PE is the decarboxylation of PS. The contributions of the two pathways to the cellular pattern of PE are organism and cell-type dependent. PS decarboxylation is actually the sole route for PE biosynthesis in *E. coli* (Kanfer and Kennedy, 1963) and the major one in *S. cerevisiae*, although in yeast the Kennedy pathway is also active (Dowhan, 1997). In mammalian cells, the relative contributions of these pathways to PE formation is cell-type dependent, with PS decarboxylation prevailing in BHK21 and CHO cells and the Kennedy pathway prevailing in most mammalian tissues, and cultured glioma cells (Vance, 2008) (Fig. 7A).

The relative contribution of the PS decarboxylation pathway to PE in BSF *T. brucei* has been assessed by us using stable isotope labelling, with d_3-serine and subsequent analysis by ESI-MS/MS (Gibellini *et al*. 2009). The d_3-serine is readily incorporated into d_3-PS, but it was unable to form any d_3-PE from d_3-PS via decarboxylation – thus highlighting the importance of the Kennedy pathway in the biosynthesis of PE in bloodstream-form *T. brucei* (Gibellini *et al*. 2008). This was confirmed by the genetic validation, via a conditional knockout, of the ECT gene in which PS decarboxylation was not unregulated to compensate for the loss of the *de novo* synthesized PE (Gibellini *et al*. 2009). These findings are in contradiction with previous work (Menon *et al*. 1993; Rifkin *et al*. 1995), which indicated that bloodstream form *T. brucei* was able to synthesise PE from PS via decarboxylation. This difference may be due to variations in the experimental conditions, while the stable-isotope labelling experiments were conducted under steady-state conditions with ample levels of serine, the radiolabelling experiments were conducted over a short period of time (1 hour), as well as in serine-free media, which may trigger differential usage of the sparingly available serine which is also required for protein synthesis. One also has to consider if the freshly synthesised PS will be decarboxylated preferentially over the pre-existing pool of PS, and if it is in the correct cellular location, i.e. available to the PS decarboxylase.

Despite our lack of observable PS decarboxylase activity, preliminary results from the laboratory suggest that the putative *T. brucei* PS decarboxylase gene (Tb09.211.1610) appears to be essential in the bloodstream form of the parasite (T. K. Smith, unpublished observations).

In procyclic forms, decarboxylation of PS to PE occurs to a limited extent but it is insufficient to compensate for the disruption of the CDP-ethanolamine branch of the Kennedy pathway (Signorrell *et al*. 2008). Together, these findings raise the question, what is the role/function of the PS decarboxylase? Possibly it is highly regulated and/or has a very specific, but as yet unknown function.

The absence of the PE methylation pathway and the irrelevance of PS decarboxylation as a contributor to the steady-state molecular composition of PE, indicate that phospholipid metabolism and its regulation are different and less complex in BSF *T. brucei* (Fig. 7), than in higher eukaryotes including man. *T. brucei* selectively carries out PC and PE formation *via* the CDP-choline and CDP-ethanolamine branches of the Kennedy pathway (Gibellini *et al*. 2008), whereas in yeast, PC and PE are synthesised primarily by PE methylation and PS decarboxylation (Carman and Han, 2009); that is, pathways involving CDP-DAG. Also, in mammalian cells, PS decarboxylation is a major route for PE biosynthesis (Vance, 2008) and PE methylation activity is abundant in hepatocytes (Walkey *et al*. 1998). The less convoluted interconnections between phospholipid biosynthetic pathways make the African trypanosome a desirable system for studying lipid metabolism and the fluxes required to maintain lipid homeostatis (Fig. 7B). At the same time the absence of alternative 'salvage' routes for the biosynthesis of PC and PE renders both branches of the Kennedy pathway attractive potential drug targets. Recently we have genetically validated the ethanolamine branch of the Kennedy pathway as a drug target (Gibellini *et al*. 2009), and preliminary data on genetic validation of the choline kinase (Young, Gibellini and Smith, unpublished observations), suggests the choline branch of the Kennedy pathway could also be successfully targeted.

Inositol PL composition

PI molecular species were detected from precursor ion scanning for *m/z* 241 in negative ion mode (Fig. S5A and B, Tables S7 and S8, see Appendix). There are significant differences in the inositol PL composition of PCF and BSF trypanosomes (Fig. 8). In PCFs, the largest peak area is composed of molecular species in the 36:y series of PI whereas in BSFs it is the 40:y series. Daughter ion scanning showed that the 40:y series is mostly made up of PI (18:0/22:4–22:6). The significant decline of these molecular species in PCF cells could reflect the significant decrease in demand to synthesise

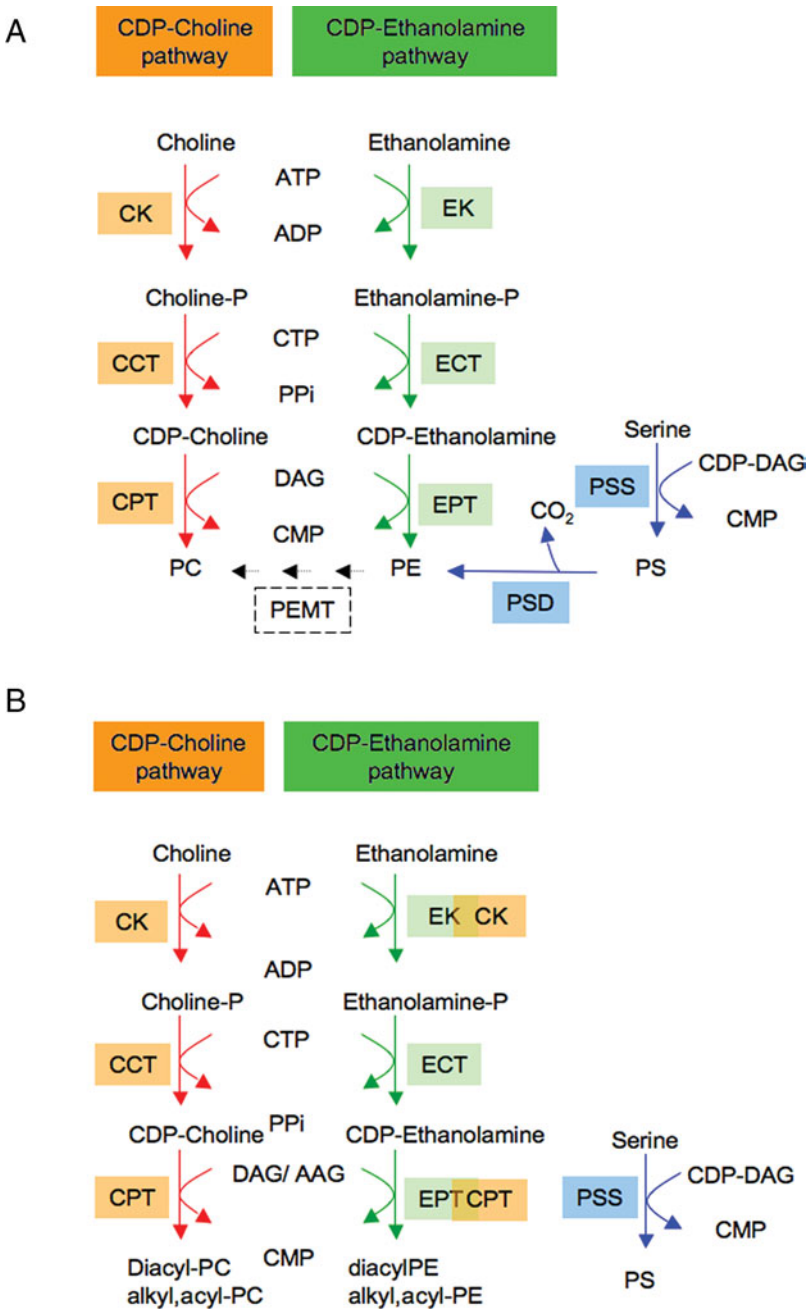

Fig. 7. *De novo* synthesis of PE, PS and PC in mammals (A) and *T. brucei* (B). Intermediates: Cho, choline; Cho-P, phosphocholine; CDP-Cho, cytidine-diphosphocholine; PC, phosphatydylcholine; Etn, ethanolamine; Etn-P, phosphoethanolamine; CDP-Etn, cytidine-diphosphoethanolamine; PE, phosphatidylethanolamine; DAG, diacylglycerol; AAG, alkylacylglycerol. Enzymes: CK, choline kinase (Tb927.5.1140); CCT, phosphocholine cytidylyltransferase (Tb10.389.0730); CPT, choline phosphotransferase (Tb10.389.0730, Tb10.6k15.1570); EK, ethanolamine kinase (Tb11.18.0017, Tb927.5.1140); ECT, phosphoethanolamine cytidylyltransferase (Tb11.01.5730); EPT, ethanolamine phosphotransferase (Tb10.389.01-40, Tb 10.6k15.1570); PSD, phosphatidylserine decarboxylase (Tb09.211.1610); PSS, phosphatidylserine synthase.

glycosylphosphatidylinositol in this form of the parasite compared to BSF cells, as well as the formation of inositol phosphoceramide (IPC) in PCF, which varies in amounts from 5–15% of total inositol PLs (Fig. 8). Furthermore, diacyl and ether PI species containing shorter FAs were present in PCF PI (Fig. S5A and B, Tables S7 and S8, see Appendix), whereas these molecular species and IPC were not detected in the BSF analysis.

It was previously thought that BSF trypanosomes only contained diacyl PI (Patnaik *et al*. 1993), but the data generated from this study showed that the diacyl subclass constitutes 80% and 90% of total PI in PCF and BSF trypanosomes, respectively, and that ether

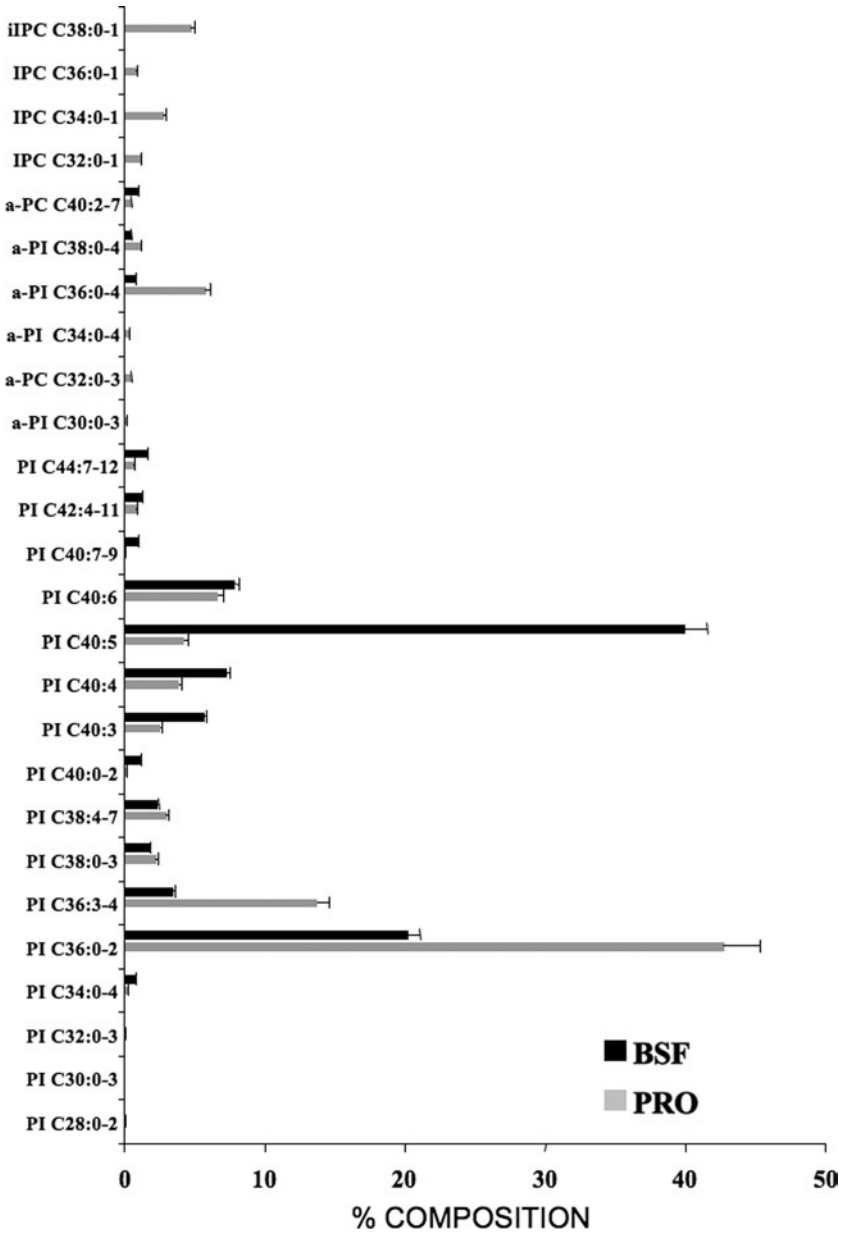

Fig. 8. Molecular composition of inositol-containing PLs in *T. brucei*. Precursor ion scanning for *m/z* 241 specifically detected $[M-H]^-$ PI and IPC ions from PCF and BSF trypanosome total lipid extracts, see Fig. S5. Molecular species are plotted against their relative percentage based upon TIC, PCF (BLACK) and BSF (GREY). Peak assignments are based on MS-MS daughter ion spectra performed as stated in the Material and Methods section, and each peak series is annotated by a letter, which are annotated in Tables S7 and S8.

lipids are certainly present in both PCF and BSF cells (Fig. 8).

Despite IPC being a major sphingolipid in other trypanosomatids (Kaneshiro *et al*. 1986; Bertello *et al*. 1995; Uhrig *et al*. 1996; Zhang *et al*. 2007), and it being observed previously in PCF *T. brucei* (Güther *et al*. 2008), its role remians unclear. However, IPC has been observed at high concentrations (~50% of the total inositol PLs) in purified mitochondria (Güler *et al*. 2006), suggesting a significant role/synthesis in this organelle. Interestly, we have also recently observed IPC formation in stumpy BSF, and this has been associated with the up-regulation of one of the four sphingomyelin synthases responsible for IPC formation (Kabani *et al*. 2009; Milna *et al*. 2009).

Other acidic PLs

PA, which is an important molecule in protein and membrane transport, has the simplest polar head-group (a phosphate) among the PL classes and readily forms $[M-H]^-$ ions. As in other eukaryotic cells PA is present in only modest quantities in *T. brucei*, and it can only be detected by precursor ion scanning for *m/z* 153 in negative ion mode, which detects negative ions from all glycerophospholipids (Fig. S6, see Appendix). Detection of lyso-PA $[M-H]^-$ and

its associated FA ions formed from collision-induced dissociation of PA $[M-H]^-$ ions confirmed its presence among the more abundant PLs. The molecular species variation among PA appears to be very similar to the species distribution of the other PLs, and they exist as both diacyl and ether lipid subclasses (Fig. 5). As with the other PLs in *T. brucei*, some PA contains long-chain highly unsaturated molecular species, which by MS-MS showed to be mostly PA (16:0/22:6) (719 m/*z*), PA (16:0/22:5) (721 m/*z*), PA (18:0/22:6) (747 m/*z*) and PA (18:0/22:5) (749 m/*z*).

PG is also a minor component in both BSF and PCF *T. brucei* membranes and the neutral headgroup of PG precludes its specific detection but it can be most easily detected with other PLs by scanning for *m*/*z* 153 in negative ion mode (Fig. S6, see Appendix). Collision-induced decomposition of 757, 759 and 809 m/*z* showed that ether PG is also present in these cells. PG is also a minor component in both BSF and PCF *T. brucei* membranes and serves as a precursor for the synthesis of cardiolipin, which is an essential lipid component of mitochondria *T. brucei* membranes (Dixon and Williamson, 1970) where it maintains the membrane potential. Previously we have also observed cardolipin species in purified PCF mitochondria (Güler *et al*. 2008), along with several other phospholipids including very minor amounts of ethanolamine phosphoceramide (Sutterwala *et al*. 2008), and significant amounts of PIP_2 and PIP_3. (T. K. Smith, unpublished observation). These will be discussed and fully characterized in subsequent work on the lipidomes of individual organelles from *T. brucei* and other protozoa.

CONCLUSION

MS technology adapted to nanoflow mode has made it possible to efficiently detect all the major *T. brucei* PLs in one liquid sample of total lipid extract. Overall, the results presented here for the composition of diacyl PC, PE and PI agree with those obtained using older methods that were not suitable for routine analysis. In addition, we have elucidated for the first time the molecular species composition for PS, PA and PG. These analyses also show that the *T. brucei* PL pools exhibit greater heterogeneity in their alkyl-acyl and alkenylacyl species than previously thought. The most significant contrast between PCF and BSF PL composition is the inositol-containing PLs, i.e. the formation of the non-mammalian like sphingolipid IPC, in the PCF.

Though relatively little information is still known about lipid biosynthesis in *T. brucei* and other kinetoplastids, the remarkable variation in PL molecular species and the large quantities of HUFAs present in *T. brucei* PLs testify to the competency of this obligate parasite to control its own fatty acid and thus lipid composition despite being reliant upon lipid precursors from its hosts.

The simplified aminophospholipid metabolism, i.e. the lack of interconversion of PS to PE to PC, is in direct contrast to that in humans and other mammals (compare Fig. 7A and B). This puts the parasite at a distinct disadvantage, as it also appears that these *de novo* pathways are essential and thus contain promising drug targets. The lack of cross-talk between these *de novo* phospholipid pathways also makes *T. brucei* an ideal organism in which to study metabolic fluxes in these pathways.

ACKNOWLEDGEMENTS

We also wish to acknowledge access to the mass spectrometry facilities both at the University of St Andrews and the University of Dundee.

FINANCIAL SUPPORT

Research in the author's laboratory is supported in part by a Wellcome Trust Senior Research Fellowship (067441), and Wellcome Trust project grant (086658) and studentships from the Wellcome Trust, BBSRC and SUSLA.

ABBREVIATIONS

PC, phosphatidylcholine; PE, phosphatidylethanolamine; PS, phosphatidylserine; PI, phosphatidylinositol; PA, phosphatidic acid; PG, phosphatidylglycerol; lyso-PC, lysophosphatidylcholine; IPC, inositol phosphoceramide; SM, sphingomyelin; PL, phospholipid; FA, fatty acid; PCF, procyclic form; BSF, bloodstream form.

REFERENCES

Bertello, L., Goncalvez, M. F., Colli, W. and de Lederkremer, R. M. (1995). Structural analysis of inositol phospholipids from *Trypanosoma cruzi* epimastigote forms. *Biochemical Journal* **310**, 255–261.

Bligh, E. G. and Dyer, W. J. (1959). A rapid method of total lipid extraction and purification. *Canadian Journal of Biochemistry and Physiology* **37**, 911–917.

Brugger, B., Erben, G., Sandhoff, R., Wieland, F. T. and Lehmann, W. D. (1997). Quantitative analysis of biological membrane lipids at the low picomole level by nano-electrospray ionization tandem mass spectrometry. *Proceedings of the National Academy of Sciences, USA* **94**, 2339–2344.

Buxbaum, L. U., Milne, K. G., Werbovetz, K. A. and Englund, P. T. (1996). Myristate exchange on the *Trypanosoma brucei* variant surface glycoprotein. *Proceedings of the National Academy of Sciences, USA* **93**, 1178–1183.

Buxbaum, L. U., Raper, J., Opperdoes, F. R. and Englund, P. T. (1994). Myristate exchange. A second glycosyl phosphatidylinositol myristoylation reaction in African trypanosomes. *Journal of Biological Chemistry* **269**, 30212–30220.

Carman, G. M. and Han, G. S. (2009). Regulation of phospholipid synthesis in yeast. *Journal of Lipid Research* **50S**, S69–S73.

Chilton, F. H. 3rd and Murphy, R. C. (1986). Fast atom bombardment analysis of arachidonic acid-containing phosphatidylcholine molecular species. *Biomedical and Environmental Mass Spectrometry* **13**, 71–76.

Denny, P. W., Goulding, D., Ferguson, M. A. and Smith, D. F. (2004). Sphingolipid-free *Leishmania* are defective in membrane trafficking, differentiation and infectivity. *Molecular Microbiology* **52**, 313–327.

Dixon, H., Ginger, C. D. and Williamson, J. (1971). The lipid metabolism of blood and culture forms of *Trypanosoma lewisi* and *Trypanosoma rhodesiense*. *Comparative Biochemistry and Physiology Part B* **39**, 247–266.

Dixon, H. and Williamson, J. (1970). The lipid composition of blood and culture forms of *Trypanosoma lewisi* and *Trypanosoma rhodesiense* compared with that of their environment. *Comparative Biochemistry and Physiology* **33**, 111–128.

Dowhan, W. (1997). Molecular basis for membrane phospholipid diversity: Why are there so many lipids? *Annual Reviews of Biochemistry* **66**, 199–232.

Fadok, V. A., de Cathelineau, A., Daleke, D. L., Henson, P. M. and Bratton, D. L. (2001). Loss of phospholipid asymmetry and surface exposure of phosphatidylserine is required for phagocytosis of apoptotic cells by macrophages and fibroblasts. *Journal of Biological Chemistry* **276**, 1071–1077.

Fahy, E., Subramaniam, S., Brown, H. A., Glass, C. K., Merrill, A. H. Jr., Murphy, R. C., Raetz, C. R., Russell, D. W., Seyama, Y., Shaw, W., Shimizu, T., Spener, F., van Meer, G., Van Nieuwenhze, M. S., White, S. H., Witztum, J. L. and Dennis, E. A. (2005). A comprehensive classification system for lipids. *Journal of Lipid Research* **46**, 839–861.

Fridberg, A., Olsen, C. L., Nakayasu, E. S., Tyler, K. M., Almeida, I. C. and Engman, D. M. (2008). Sphingolipid synthesis is necessary for kinetoplast segregation and cytokinesis in *Trypanosoma brucei*. *Journal of Cell Science* **121**, 522–535.

Gibellini, F., Hunter, W. N. and Smith, T. K. (2008). Biochemical characterisation of the initial steps of the Kennedy pathway in *Trypanosoma brucei* – the ethanolamine and choline kinases. *Biochemical Journal* **415**, 135–144.

Gibellini, F., Hunter, W. N. and Smith, T. K. (2009). The ethanolamine branch of the Kennedy pathway is essential in the bloodstream form of *Trypanosoma brucei*. *Molecular Microbiology* **73**, 826–843.

Gibellini, F. and Smith, T. K. (2010). The Kennedy Pathway - *de novo* synthesis of phosphatidylethanolamine and phosphatidylcholine. *IUBMB Life* (in press). doi:10.1002/ivb.337

Godfrey, D. G. (1967). Phospholipids of *Trypanosoma lewisi, T. vivax, T.* congolense, and *T. brucei*. *Experimental Parasitology* **20**, 106–118.

Güler, J. L., Kriegová, E., Smith, T. K., Luke, J. and Englund, P. T. (2008). Mitochondrial fatty acid synthesis is required for normal mitochondrial morphology and function in *Trypanosoma brucei*. *Molecular Microbiology* **67**, 1125–1142.

Güther, M. L. S., Lee, S., Tetley, L., Acosta-Serrano, A. and Ferguson, M. A. J. (2006). GPI anchored proteins and free GPI glycolipids of procyclic form *Trypanosoma brucei* are non-essential for growth, are required for colonization of the tsetse fly and are not the only components of the surface coat. *Molecular Biology of the Cell* **17**, 5265–5274.

Ishii, I., Fukushima, N., Ye, X. and Chun, J. (2004). Lysophospholipid receptors: signaling and biology. *Annual Review of Biochemistry* **73**, 321–354.

James, S. R. and Downes, C. P. (1997). Structural and mechanistic features of phospholipases C: effectors of inositol phospholipid-mediated signal transduction. *Cell Signal* **9**, 329–336.

Kabani, S., Fenn, K., Ross, A., Ivens, A., Smith, T. K., Ghazal, P. and Matthews, K. (2009). Genome-wide expression profiling of *in vivo*-derived bloodstream parasite stages and dynamic analysis of mRNA alterations during synchronous differentiation in *Trypanosoma brucei*. *BMC Genomics* **10**, 427–441.

Kaneshiro, E. S., Jayasimhulu, K. and Lester, R. L. (1986). Characterization of inositol lipids from *Leishmania donovani* promastigotes: identification of an inostiol sphingophospholipid. *Journal of Lipid Research* **27**, 1294–1303.

Kanfer, J. and Kennedy, E. P. (1963). Metabolism and function of bacterial lipids. *Journal of Biological Chemistry* **238**, 2919–2922.

Kennedy, E. P. and Weiss, S. B. (1956). The function of cytidine coenzymes in the biosynthesis of phospholipids. *Journal of Biological Chemistry* **222**, 193–214.

Kerwin, J. L., Tuininga, A. R. and Ericsson, L. H. (1994). Identification of molecular species of glycerophospholipids and sphingomyelin using electrospray mass spectrometry. *Journal of Lipid Research* **35**, 1102–1114.

Le Roch, K. G., Johnson, J. R., Ahiboh, H., Chung, D.-W. D., Prudhomme, J. and Plouffe, D. (2008). A systematic approach to understand the mechanism of action of the bisthiazolium compound T4 on the human malaria parasite, *Plasmodium falciparum*. *BMC Genomics* **9**, article no. 513.

Martin, K. L. and Smith, T. K. (2006*a*). Phosphatidylinositol synthesis is essential in bloodstream form *Trypanosoma brucei*. *Biochemical Journal* **396**, 287–295.

Martin, K. L. and Smith, T. K. (2006*b*). The glycosylphosphatidylinositol (GPI) biosynthetic pathway of bloodstream-form *Trypanosoma brucei* is dependent on the *de novo* synthesis of inositol. *Molecular Microbiology* **61**, 89–105.

Menon, A. K., Eppingerl, M., Mayor, S. and Schwarz, R. (1993). Phosphatidylethanolamine is the donor of the phosphoethanolamine group in trypanosome glycosyl-phosphatidylinositol. *EMBO Journal* **12**, 1907–1914.

Michels, P. A., Hannaert, V. and Bringaud, F. (2000). Metabolic aspects of glycosomes in trypanosomatidae – new data and views. *Parasitology Today* **16**, 482–489.

Milna, J. G., Pan, S. Y., Wansadhipathi, N. K., Bruce, C. R., Shams-Eldin, H., Schwarz, R. T., Steel, P. G. and Denny, P. W. (2009). The *Trypanosoma brucei* sphingolipid synthase, an essential enzyme and drug target. *Molecular and Biochemical Parasitology* **168**, 16–23.

Overath, P. and Engstler, M. (2004). Endocytosis, membrane recycling and sorting of GPI-anchored proteins: *Trypanosoma brucei* as a model system. *Molecular Microbiology* **53**, 735–744.

Patnaik, P. K., Field, M. C., Menon, A. K., Cross, G. A., Yee, M. C. and Butikofer, P. (1993). Molecular species analysis of phospholipids from *Trypanosoma brucei* bloodstream and procyclic forms. *Molecular and Biochemical Parasitology* **58**, 97–105.

Pessi, G., Choi, J. Y., Reynolds, J. M., Voelker, D. R. and Mamoun, C. B. (2005). *In vivo* evidence for the specificity of *Plasmodium falciparum* phosphoethanolamine methyltransferase and its coupling to the Kennedy pathway. *Journal of Biological Chemistry* **280**, 12461–12466.

Richmond, G. S. and Smith, T. K. (2007*a*). The role and characterization of phospholipase A1 in mediating lysophosphatidylcholine synthesis in *Trypanosoma brucei*. *Biochemical Journal* **405**, 319–329.

Richmond, G. S. and Smith, T. K. (2007*b*). A novel phospholipase from *Trypanosoma brucei*. *Molecular Microbiology* **63**, 1078–1095.

Rifkin, M. R., Strobos, C. A. M. and Fairlamb, A. H. (1995). Specificity of ethanolamine transport and its further metabolism in *Trypanosoma brucei*. *Journal of Biological Chemistry* **270**, 16160–16166.

Signorell, A., Rauch, M., Jelk, J., Ferguson, M. A. J. and Bütikofer, P. (2008) Phosphatidylethanolamine in *Trypanosoma brucei* is organized in two separate pools and is synthesized exclusively by the Kennedy Pathway. *Journal of Biological Chemistry* **283**, 23636–23644.

Six, D. A. and Dennis, E. A. (2000). The expanding superfamily of phospholipase A(2) enzymes: classification and characterization. *Biochimica et Biophysica Acta* **1488**, 1–19.

Smith, J. D. (1993). Phospholipid biosynthesis in protozoa. *Progress in Lipid Research* **32**, 47–60.

Smith, T. K. and Bütikofer, P. (2010). Phospholipid biosynthesis in *Trypansoma brucei*. *Molecular Biochemical Parasitology* (in press). doi:10.1016/j.molbiopara.2010.04.01

Sutterwala, S. S., Creswell, C. H., Sanyal, S., Menon, A. K. and Bangs, J. D. (2007). *De novo* sphingolipid synthesis is essential for viability, but not transport of glycosylphosphatidylinositol-anchored proteins in African trypanosomes. *Eukaryotic Cell* **6**, 454–464.

Sutterwala, S. S., Hsu, F. F., Sevova, E. S., Schwartz, K. J., Zhang, K., Key, P., Turk, J., Beverley, S. M. and Bangs, J. D. (2008). Developmentally regulated sphingolipid synthesis in African trypanosomes. *Molecular Microbiology* **70**, 281–296.

Uhrig, M. L., Couto, A. S., Colli, W. and de Lederkremer, R. M. (1996). Characterization of inositolphospholipids in *Trypanosoma cruzi* trypomastigote forms. *Biochimica et Biophysica Acta* **1300**, 233–239.

Urbina, A. J. (2006). Mechanisms of action of lysophospholipid analogues against trypanosomatid parasites. *Transactions of the Royal Society of Tropical Medicine and Hygiene* **100**, S9–S16.

van Hellemond, J. J. and Tielens, A. G. (2006). Adaptations in the lipid metabolism of the protozoan parasite *Trypanosoma brucei*. *FEBS Letters* **580**, 5552–5558.

Vance, J. E. (2008). Phosphatidylserine and phosphatidylethanolamine in mammalian cells: two metabolically related aminophospholipids. *Journal of Lipid Research* **49**, 1377–1387.

Venkatesan, S. and Ormerod, W. E. (1976). Lipid content of the slender and stumpy forms of *Trypanosoma brucei rhodesiense:* a comparative study. *Comparative Biochemistry and Physiology Part B* **53**, 481–487.

Vial, H. J., Eldin, P., Tielens, A. G. and van Hellemond, J. J. (2003). Phospholipids in parasitic protozoa. *Molecular and Biochemical Parasitology* **126**, 143–154.

Voncken, F., van Hellemond, J. J., Pfisterer, I., Maier, A., Hillmer, S. and Clayton, C. (2003). Depletion of GIM5 causes cellular fragility, a decreased glycosome number, and reduced levels of ether-linked phospholipids in trypanosomes. *Journal of Biological Chemistry* **278**, 35299–35310.

Walkey, C. J., Yu, L., Agellon, L. B. and Vance, D. E. (1998). Biochemical and evolutionary significance of phospholipid methylation. *Journal of Biological Chemistry* **273**, 27043–27046.

Wirtz, E., Leal, S., Ochatt, C. and Cross, G. A. (1999). A tightly regulated inducible expression system for conditional gene knock-outs and dominant-negative genetics in *Trypanosoma brucei*. *Molecular and Biochemical Parasitology* **99**, 89–101.

Zachowski, A. (1993). Phospholipids in animal eukaryotic membranes: transverse asymmetry and movement. *Biochemical Journal* **294**, 1–14.

Zhang, K., Pompey, J. M., Hsu, F.-F., Key, P., Bandahuvula, P. and Saba, J. D. (2007). Redirection of sphingolipid metabolism towards *de novo* synthesis of ethanolamine in *Leishmania*. *EMBO Journal* **26**, 1094–1104.

Zufferey, R., Allen, S., Barron, T., Sullivan, D. R., Denny, P. W., Almeida, I. C., Smith, D. F., Turco, S. J., Ferguson, M. A. and Beverley, S. M. (2003). Ether phospholipids and glycosylinositolphospholipids are not required for amastigote virulence or for inhibition of macrophage activation by *Leishmania major*. *Journal of Biological Chemistry* **278**, 44708–44718.

APPENDIX 1. SUPPLEMENTARY DATA

Table S1. Mass spectrometry analysis of PC and SM molecular species in the procyclic form of *T. brucei*

Peak[a]	*HR m/z*[b]	Lipid component[c]	Principal component[d]	*Theor m/z*[e]
A′ (0·2%)				
1	520·28	18:2	0:0/18:2	520·3398
2	522·30	18:1	0:0/18:1	522·3554
3	524·34	18:0	0:0/18:0	524·3711
B′				
4	544·33	20:4	0:0/20:4	544·3398
5	546·34	20:3	0:0/20:3	546·3554
6	548·34	20:2	0:0/20:2	548·3711
C′ (0·2%)				
7	568·35	22:6	0:0/22:6	568·3398
8	570·38	22:5	0:0/22:5	570·3554
9	572·38	22:4	0:0/22:4	572·3711
D′				
10	646·44	26:2	0:0/26:2	646·4443
11	648·46	26:1	0:0/26:1	648·4599
12	650·48	26:0	0:0/26:0	650·4756
E′				
13	660·60	a-28:2	a-14:0/14:2	660·5363
14	663·57	a-28:1	a-14:0/14:1	662·5119
15	664·54	a-28:0	a-14:0/14:0	664·5276
A (0·3%)				
16	674·47	28:2	14:0/14:2	674·4756
17	676·51	28:1	14:0/14:2	676·4912
18	675·53	SM(14:0)	Cer d18:0/14:1	676·5541
19	878·51	28:0	14:0/14:0	678·5069
B (0·1%)				
20	686·33	e-30:2	e-14:1/16:2	686·5220
21	686·48	e-30:1, a-30:2	a-14:0/16:2	688·5376
22	690·53	e-30:0, a-30:1	a-14:0/16:1	690·5432
23	692·52	a-30:0	a-14:0/16:0	692·5589
C (0·4%)				
24	698·50	30:4	16:2/14:2	698·4756
25	700·53	30:3	16:2/14:1	700·4912
26	703·56	30:2	16:0/14:2	703·5169
27	704·61	SM (16:0)	Cer d18:0/16:1	704·5851
28	704·57	30:1	16:0/14:1	704·5225
29	706·55	30:0	16:0/14:0	706·5382
D (0·2%)				
30	716·59	e-32:1, a-32:2	e-16:1/16:1	716·5589
31	718·58	e-32:0, a-32:1	e-16:1/16:0	718·5745
32	720·60	a-32:0	a-16:0/16:0	720·5902
E (1·8%)				
33	728·52	32:3	16:1/16:2	728·5225
34	730·53	32:2	16:0/16:2	730·5382
35	732·55	32:1	16:0/16:1	732·5538
36	732·61	SM(18:0)	Cer d18:0/18:1	732·6167
37	734·59	32:0	16:0/16:0	734·5695
F (1·5%)				
38	738·54	e-34:4, a-34:5	a-14:0/20:5	738·5433
39	740·58	e-34:3, a-34:4	a-14:0/20:4	740·5589
40	742·57	e-34:2, a-34:3	a-14:0/20:3	742·5745
41	744·60	e-34:1, a-34:2	a-16:0/18:2	744·5902
42	746·61	e-34:0, a-34:1	a-16:0/18:1	746·6058
43	748·61	a-34:0	a-16:0/16:0	748·6215
G (3·9%)				
44	754·54	34:4	16:2/18:2	754·5382
45	756·55	34:3	16:1/18:2	756·5538
46	758·57	34:2	16:0/18:2	758·5695
47	759·62	SM(20:0)	Cer18:1/20:0	759·6401

Table S1. (*Cont.*)

Peak[a]	*HR m/z*[b]	Lipid component[c]	Principal component[d]	*Theor m/z*[e]
48	760·59	34:1	16:0/18:1	760·5851
49	762·62	34:0	16:0/18:0	762·6008
H (12·5%)				
50	766·58	e-36:4, a-36:5	e-16:1/20:4	766·5745
51	768·57	e-36:3, a-36:4	a-16:0/20:4	768·5902
52	**770·61**	**e-36:2, a-36:3**	**e-18:1/18:2**	**770·6058**
53	**772·64**	**e-36:1, a-36:2**	**a-18:0/18:2**	**772·6215**
54	**774·63**	**e-36:0, a-36:1**	**a-18:0/18:1**	**774·6371**
55	776·62	a-36:0	a-18:0/18:0	776·6528
I (20·8%)				
56	778·55	36:6	16:2/20:4	778·5382
57	780·54	36:5	16:1/20:4	780·5538
58	782·55	36:4	16:0/20:4	782·5695
59	**784·56**	**36:3**	**18:1/18:2**	**784·5851**
60	**786·60**	**36:2**	**18:0/18:2 & 18:1/18:1**	**786·6008**
61	**788·57**	**36:1**	**18:0/18:1**	**788·6164**
62	**789·64**	**SM(22:0)**	**Cer18:0/22:0**	**789·68**
64	790·60	36:0	18:0/18:0	790·6321
J (1·7%)				
63	790·54	e-38:6	e-16:1/22:6	790·5745
65	792·57	e-38:5, a-36:6	a-16:0/22:6	792·5902
66	794·54	e-38:4, a-38:5	e-18:1/20:4	794·5695
67	796·84	e-38:3, a-38:4	a-18:0/20:4	796·6215
68	798·64	e-38:2, a-38:3	e-18:1/20:2	798·6371
69	800·68	e-38:1, a-38:2	a-18:0/20:2	800·6528
70	802·68	e-38:0, a-38:1	a-18:0/20:1	802·6684
71	804·54	38:7	16:1/22:6	804·5538
72	804·69	a-38:0	a-18:0/20:0	804·6841
K (9·7%)				
73	**806·53**	**38:6**	**16:0/22:6**	**806·5695**
74	**808·53**	**38:5**	**16:0/22:5**	**808·5851**
75	**810·59**	**38:4**	**18:0/20:4 & 16:0/22:4**	**810·6008**
76	**812·61**	**38:3**	**18:0/20:3**	**812·6164**
77	**814·64**	**38:2**	**18:0/20:2**	**814·6321**
78	816·64	38:1	18:0/20:1	816·6477
79	818·68	38:0	18:0/20:0	818·6634
L (1·5%)				
80	818·58	e-40:6	e-18:1/22:6	818·6058
81	820·63	e-40:5, a-40:6	a-18:0/22:6	820·6215
82	822·64	e-40:4, a-40:5	e-18:1/22:4	822·6371
83	824·65	e-40:3, a-40:4	a-18:0/22:4	824·6528
84	826·64	e-40:2, a-40:3	e-18:1/22:2	826·6321
85	828·67	e-40:1, a-40:2	a-18:0/22:2	828·6841
86	830·69	e-40:0, a-40:1	e-18:1/22:0	830·6997
87	832·72	a-40:0	a-18:0/22:0	832·7154
M (36·1%)				
88	**830·56**	**40:8**	**18:2/22:6**	**830·5695**
89	**832·58**	**40:7**	**18:1/22:6**	**832·5851**
90	**834·61**	**40:6**	**18:0/22:6**	**834·6008**
91	**836·61**	**40:5**	**18:0/22:5**	**836·6164**
92	**838·63**	**40:4**	**18:2/22:4**	**838·6321**
93	**840·65**	**40:3**	**18:1/22:2**	**840·6477**
94	**842·67**	**40:2**	**18:0/22:2**	**842·6634**
95	844·71	40:1	18:1/22:0	844·6790
96	846·72	40:0	18:0/22:0	846·6947
97	848·68	e-42:6	e-18:1/24:6	848·6528
98	850·69	e-42:5	e-18:1/24:4	850·6684
99	852·70	a-42:4	a-18:0/24:4	852·6841
N (4·6%)				
101	852·59	42:11	20:4/22:5	852·5538
102	854·72	a-42:3	e-18:1/24:2	854·6997
103	854·57	42:10	20:4/22:6	854·5695
104	856·73	a-42:2	a-18:0/24:2	856·7154
105	856·61	42:9	20:4/22:5	856·5851

Table S1. (*Cont.*)

Peak[a]	*HR m/z*[b]	Lipid component[c]	Principal component[d]	*Theor m/z*[e]
106	858·75	a-42:1	a-18:1/24:0	858·7310
107	858·60	42:8	18:2/24:6	858·6008
108	860·61	42:7	18:1/24:6	860·6164
109	860·73	a-42:0	a-18:0/24:0	860·7467
110	862·64	42:6	18:0/24:6	862·6321
111	864·65	42:5	18:0/24:5	864·6477
112	866·66	42:4	18:2/24:4	866·6634
113	868·67	42:3	18:1/24:2	868·6790
114	870·72	42:2	18:0/24:2	870·6947
115	872·73	42:1	18:1/24:0	872·7103
116	874·74	42:0	18:0/24:0	874·7260
O (4·4%)				
117	878·58	44:12	20:6/24:6	878·5695
118	852·59	44:11	20:6/24:5	852·5565
119	882·59	44:10	20:4/24:6	882·6008
120	886·62	44:8	20:4/24:4	886·6321
121	888·63	44:7	20:2/24:5	888·6477
122	890·64	44:6	20:1/24:6	890·6634
123	892·65	44:5	20:0/24:5	892·6790
124	894·66	44:4	18:0/26:4	894·6947
125	896·67	44:3	20:1/24:2	896·7103
126	898·70	44:2	20:0/24:2	898·7260
127	900·71	44:1	18:0/26:1	900·7416
128	902·72	44:0	18:0/26:0	902·7573

[a] All of the molecular species detected within a series are grouped by a letter are contained within the lowest and highest mass range and refers to the corresponding peaks in Fig. 4A. The percentages in parentheses correspond to the relative percentage based upon TIC. The peaks containing the most abundant PC/SM species are in bold.

[b] HR $[M+H]^+$ ions, mass over charge values (high resolution survey scan) ±0·05 m/z were obtained as described in Materials and Methods.

[c] Peak identities refer to total number of carbon atoms and double bonds. e = plasmenyl (alkenylacyl); a = plasmanyl (alkylacyl).

[d] Precise fatty acyl constituents and their positions are not discernable in positive ion mode; however, where possible, the most likely fatty acid candidates for the *sn*-1 and *sn*-2 constituents of the molecular species presented were deduced from the available literature. Only the principal component is given, in some instances as many as 5 individual species, with different combinations of acyl chains result in the same total number of carbon atoms and double bonds.

[e] Theoretical monoisotopic masses were obtained were possible for LIPIDMAPS, otherwise they were calculated using http://www.sisweb.com/referenc/tools/exactmass.htm.

Table S2. Mass spectrometry analysis of PC and SM molecular species in the bloodstream form of *T. brucei*

Peak[a]	*HR m/z*[b]	Lipid component[c]	Principal component[d]	*Theor m/z*[e]
A′				
1	520·30	18:2	0:0/18:2	520·3398
2	522·31	18:1	0:0/18:1	522·3554
3	524·33	18:0	0:0/18:0	524·3711
B′				
4	544·34	20:4	0:0/20:4	544·3398
5	546·32	20:3	0:0/20:3	546·3554
6	548·37	20:2	0:0/20:2	548·3711
C′				
7	568·35	22:6	0:0/22:6	568·3398
8	570·37	22:5	0:0/22:5	570·3554
9	572·37	22:4	0:0/22:4	572·3711
D′				
10	646·45	26:2	0:0/26:2	646·4443
11	648·47	26:1	0:0/26:1	648·4599
12	650·49	26:0	0:0/26:0	650·4756
E′				
13	660·59	a-28:2	a-14:0/14:2	660·5363
14	663·55	a-28:1	a-14:0/14:1	662·5119
15	664·51	a-28:0	a-14:0/14:0	664·5276
A (0·2%)				
16	674·49	28:2	14:0/14:2	674·4756
17	676·52	28:1	14:0/14:2	676·4912
18	675·52	SM(14:0)	Cer d18:0/14:1	676·5541
19	878·53	28:0	14:0/14:0	678·5069
B (0·2%)				
20	686·32	e-30:2	e-14:1/16:2	686·5220
21	686·29	e-30:1, a-30:2	a-14:0/16:2	688·5376
22	690·56	e-30:0, a-30:1	a-14:0/16:1	690·5432
23	692·53	a-30:0	a-14:0/16:0	692·5589
C (0·2%)				
24	698·49	30:4	16:2/14:2	698·4756
25	700·52	30:3	16:2/14:1	700·4912
26	703·54	30:2	16:0/14:2	703·5169
27	704·62	SM (16:0)	Cer d18:0/16:1	704·5851
28	704·55	30:1	16:0/14:1	704·5225
29	706·54	30:0	16:0/14:0	706·5382
D (0·4%)				
30	716·57	e-32:1, a-32:2	e-16:1/16:1	716·5589
31	718·59	e-32:0, a-32:1	e-16:1/16:0	718·5745
32	720·62	a-32:0	a-16:0/16:0	720·5902
E (1·2%)				
33	728·54	32:3	16:1/16:2	728·5225
34	730·55	32:2	16:0/16:2	730·5382
35	732·57	32:1	16:0/16:1	732·5538
36	732·64	SM(18:0)	Cer d18:0/18:1	732·6167
37	734·58	32:0	16:0/16:0	734·5695
F (1·8%)				
38	738·58	e-34:4, a-34:5	a-14:0/20:5	738·5433
39	740·57	e-34:3, a-34:4	a-14:0/20:4	740·5589
40	742·59	e-34:2, a-34:3	a-14:0/20:3	742·5745
41	744·63	e-34:1, a-34:2	a-16:0/18:2	744·5902
42	746·63	e-34:0, a-34:1	a-16:0/18:1	746·6058
43	748·61	a-34:0	a-16:0/16:0	748·6215
G (4·8%)				
44	754·55	34:4	16:2/18:2	754·5382
45	756·57	34:3	16:1/18:2	756·5538
46	758·59	34:2	16:0/18:2	758·5695
47	759·62	SM(20:0)	Cer18:1/20:0	759·64
48	760·59	34:1	16:0/18:1	760·5851
49	762·62	34:0	16:0/18:0	762·6008

Table S2. (*Cont.*)

Peak[a]	*HR m/z*[b]	Lipid component[c]	Principal component[d]	*Theor m/z*[e]
H (13·0%)				
50	766·55	e-36:4, a-36:5	e-16:1/20:4	766·5745
51	768·55	e-36:3, a-36:4	a-16:0/20:4	768·5902
52	**770·62**	**e-36:2, a-36:3**	**e-18:1/18:2**	**770·6058**
53	**772·65**	**e-36:1, a-36:2**	**a-18:0/18:2**	**772·6215**
54	**774·63**	**e-36:0, a-36:1**	**a-18:0/18:1**	**774·6371**
55	776·63	a-36:0	a-18:0/18:0	776·6528
I (19·1%)				
56	778·55	36:6	16:2/20:4	778·5382
57	780·53	36:5	16:1/20:4	780·5538
58	782·53	36:4	16:0/20:4	782·5695
59	**784·56**	**36:3**	**18:1/18:2**	**784·5851**
60	**786·59**	**36:2**	**18:0/18:2 & 18:1/18:1**	**786·6008**
61	**788·57**	**36:1**	**18:0/18:1**	**788·6164**
62	**789·65**	**SM(22:0)**	**Cer18:0/22:0**	**789·68**
64	790·61	36:0	18:0/18:0	790·6321
J (1·4%)				
63	790·54	e-38:6	e-16:1/22:6	790·5745
65	792·57	e-38:5, a-36:6	a-16:0/22:6	792·5902
66	794·54	e-38:4, a-38:5	e-18:1/20:4	794·5695
67	796·84	e-38:3, a-38:4	a-18:0/20:4	796·6215
68	798·64	e-38:2, a-38:3	e-18:1/20:2	798·6371
69	800·68	e-38:1, a-38:2	a-18:0/20:2	800·6528
70	802·68	e-38:0, a-38:1	a-18:0/20:1	802·6684
71	804·54	38:7	16:1/22:6	804·5538
K (13·6%)				
72	804·69	a-38:0	a-18:0/20:0	804·6841
73	**806·53**	**38:6**	**16:0/22:6**	**806·5695**
74	**808·53**	**38:5**	**16:0/22:5**	**808·5851**
75	**810·58**	**38:4**	**18:0/20:4 & 16:0/22:4**	**810·6008**
76	**812·60**	**38:3**	**18:0/20:3**	**812·6164**
77	**814·62**	**38:2**	**18:0/20:2**	**814·6321**
78	816·63	38:1	18:0/20:1	816·6477
79	818·57	e-40:6	e-18:1/22:6	818·6058
80	818·67	38:0	18:0/20:0	818·6634
L (1·6%)				
81	820·61	e-40:5, a-40:6	a-18:0/22:6	820·6215
82	822·61	e-40:4, a-40:5	e-18:1/22:4	822·6371
83	824·63	e-40:3, a-40:4	a-18:0/22:4	824·6528
84	826·61	e-40:2, a-40:3	e-18:1/22:2	826·6321
85	828·68	e-40:1, a-40:2	a-18:0/22:2	828·6841
86	830·68	e-40:0, a-40:1	e-18:1/22:0	830·6997
87	832·70	a-40:0	a-18:0/22:0	832·7154
M (34·4%)				
88	**830·55**	**40:8**	**18:2/22:6**	**830·5695**
89	**832·57**	**40:7**	**18:1/22:6**	**832·5851**
90	**834·59**	**40:6**	**18:0/22:6**	**834·6008**
91	**836·59**	**40:5**	**18:0/22:5**	**836·6164**
92	**838·62**	**40:4**	**18:2/22:4**	**838·6321**
93	**840·65**	**40:3**	**18:1/22:2**	**840·6477**
94	**842·68**	**40:2**	**18:0/22:2**	**842·6634**
95	844·72	40:1	18:1/22:0	844·6790
96	846·73	40:0	18:0/22:0	846·6947
97	848·66	e-42:6	e-18:1/24:6	848·6528
98	850·66	e-42:5	e-18:1/24:4	850·6684
99	852·68	a-42:4	a-18:0/24:4	852·6841
N (3·8%)				
101	852·59	42:11	20:4/22:5	852·5538
102	854·72	a-42:3	e-18:1/24:2	854·6997
103	854·57	42:10	20:4/22:6	854·5695
104	856·73	a-42:2	a-18:0/24:2	856·7154
105	856·59	42:9	20:4/22:5	856·5851

Table S2. (*Cont.*)

Peak[a]	*HR m/z*[b]	Lipid component[c]	Principal component[d]	*Theor m/z*[e]
106	858·75	a-42:1	a-18:1/24:0	858·7310
107	858·59	42:8	18:2/24:6	858·6008
108	860·57	42:7	18:1/24:6	860·6164
109	860·72	a-42:0	a-18:0/24:0	860·7467
110	862·61	42:6	18:0/24:6	862·6321
111	864·63	42:5	18:0/24:5	864·6477
112	866·66	42:4	18:2/24:4	866·6634
113	868·69	42:3	18:1/24:2	868·6790
114	870·73	42:2	18:0/24:2	870·6947
115	872·73	42:1	18:1/24:0	872·7103
116	874·75	42:0	18:0/24:0	874·7260
O (3·0%)				
117	878·59	44:12	20:6/24:6	878·5695
118	852·58	44:11	20:6/24:5	852·5565
119	882·59	44:10	20:4/24:6	882·6008
120	886·61	44:8	20:4/24:4	886·6321
121	888·61	44:7	20:2/24:5	888·6477
122	890·62	44:6	20:1/24:6	890·6634
123	892·63	44:5	20:0/24:5	892·6790
124	894·65	44:4	18:0/26:4	894·6947
125	896·68	44:3	20:1/24:2	896·7103
126	898·70	44:2	20:0/24:2	898·7260
127	900·72	44:1	18:0/26:1	900·7416
128	902·73	44:0	18:0/26:0	902·7573

[a] All of the molecular species detected within a series are grouped by a letter are contained within the lowest and highest mass range and refers to the corresponding peaks in Fig. 4B. The percentages in parentheses correspond to the relative percentage based upon TIC. The peaks containing the most abundant PC/SM species are in bold.
[b] As in Table S1.
[c] As in Table S1.
[d] As in Table S1.
[e] As in Table S1.

Table S3. Mass spectrometry analysis of PE molecular species in procyclic *T. brucei*

Peak[a]	*HR m/z*[b]	Lipid component[c]	Principal component[d]	*Theor m/z*[e]
A (0·7%)				
1	684·36	32:3	16:1/16:2	684·4610
2	686·42	32:2	16:0/16:2	686·4766
3	688·44	32:1	16:0/16:1	688·4923
4	690·47	32:0	16:0/16:0	690·5079
B (1·5%)				
5	696·52	a-34:4	e-16:1/18:3	696·4973
6	**698·52**	**a-34:3**	**e-16:1/18:2**	**698·5130**
7	700·54	a-34:2	a-16:0/18:2	700·5286
8	702·55	a-34:1	a-16:0/18:1	702·5443
C (3·2%)				
9	710·49	34:4	16:1/18:3	710·4766
10	**712·52**	**34:3**	**16:1/18:2**	**712·4923**
11	714·54	34:2	16:0/18:2	714·5079
12	716·55	34:1	16:0/18:1	716·5236
13	718·56	34:0	16:0/18:0	718·5392
D (72·5%)				
14	724·54	a-36:5	a-18:1/18:4	724·5286
15	**726·58**	a-36:4	a-18:1/18:3	**726·5443**
16	**728·58**	**a-36:3**	**a-18:1/18:2**	**728·5599**
17	730·59	**a-36:2**	**a-18:1/18:1**	730·5756
18	732·61	a-36:1	a-18:0/18:1	732·5912
19	734·62	a-36:0	a-18:0/18:0	734·6068
E (10·9%)				
20	738·53	36:4	18:2/18:2	738·5079
21	740·55	36:3	18:1/18:2	740·5236
22	742·56	36:2	18:0/18:2	742·5392
23	**744·58**	**36:1**	**18:0/18:1**	**744·5549**
24	746·59	36:0	18:0/18:0	746·5705
F (6·3%)				
25	748·56	a-38:6	e-18:1/20:5	748·5286
26	750·56	a-38:5	e-18:1/20:4	750·5443
27	752·57	a-38:4	a-18:0/20:4	752·5599
28	**754·59**	**a-38:3**	**a-18:0/20:3**	**754·5756**
29	756·62	a-38:2	a-18:0/20:3	756·5912
30	758·63	a-38:1	a-18:0/20:2	758·6069
31	760·64	a-38:0	a-18:0/20:1	760·6225
G (1·9%)				
32	762·53	38:6	18:2/20:4	762·5079
33	764·55	38:5	18:1/20:4	764·5236
34	**766·56**	**38:4**	**18:0/20:4**	**766·5392**
35	768·57	38:3	18:0/20:3	768·5549
36	770·58	38:2	18:0/20:2	770·5705
37	772·60	38:1	18:0/20:1	772·5862
38	774·64	**38:0**	18:0/20:0	774·6018
H (0·3%)				
39	**774·57**	**e-40:6, a-40:7**	**e-18:1/22:6**	**774·5443**
40	776·59	a-40:6	a-18:1/22:5	776·5599
I (2·6%)				
41	788·54	40:7	18:2/22:5	788·5236
42	790·57	40:6	18:1/22:5	790·5392
43	**792·58**	**40:5**	**18:1/22:4**	**792·5549**
44	794·59	40:4	18:0/22:4	794·5705
45	796·61	40:3	18:1/22:2	796·5862

[a] All of the molecular species detected within a series are grouped by a letter are contained within the lowest and highest mass range and refers to the corresponding peaks in Fig. 5A. The percentages in parentheses correspond to the relative percentage based upon TIC. The peaks containing the most abundant PE species are in bold.

[b] $HR[M-H]^-$ ions mass over charge values (high resolution survey scan) ±0·05 m/z were obtained as described in Materials and Methods. (high resolution survey scan) ±0·05 m/z were obtained as described in material methods.

[c] As in Table S1.

[d] Precise fatty acyl *sn*-1 and *sn*-2 constituents were deduced from daughter ion scanning, only the principal component is given, in some instances there are as many as 5 individual species, with different combinations of acyl groups, resulting in the same total number of carbon atoms and double bonds.

[e] As in Table S1.

Table S4. Mass spectrometry analysis of PE molecular species in bloodstream *T. brucei*

Peak[a]	*HR m/z*[b]	Lipid component[c]	Principal component[d]	*Theor m/z*[e]
B (2·4%)				
1	696·50	a-34:4	e-16:1/18:3	696·4973
2	**698·51**	**a-34:3**	**e-16:1/18:2**	**698·5130**
3	700·53	a-34:2	a-16:0/18:2	700·5286
4	702·55	a-34:1	a-16:0/18:1	702·5443
C (3·5%)				
5	710·48	34:4	16:1/18:3	710·4766
6	**712·50**	**34:3**	**16:1/18:2**	**712·4923**
7	714·51	34:2	16:0/18:2	714·5079
8	716·53	34:1	16:0/18:1	716·5236
9	718·56	34:0	16:0/18:0	718·5392
D (57·8%)				
10	724·53	a-36:5	a-18:1/18:4	724·5286
11	**726·54**	a-36:4	a-18:1/18:3	**726·5443**
12	**728·56**	**a-36:3**	**a-18:1/18:2**	**728·5599**
13	730·58	**a-36:2**	**a-18:1/18:1**	730·5756
14	732·59	a-36:1	a-18:0/18:1	732·5912
15	734·60	a-36:0	a-18:0/18:0	734·6068
E (10·6%)				
16	738·51	36:4	18:2/18:2	738·5079
17	740·53	36:3	18:1/18:2	740·5236
18	742·54	36:2	18:0/18:2	742·5392
19	**744·56**	**36:1**	**18:0/18:1**	**744·5549**
20	746·57	36:0	18:0/18:0	746·5705
F (3·1%)				
21	748·54	a-38:6	e-18:1/20:5	748·5286
22	750·55	a-38:5	e-18:1/20:4	750·5443
23	752·57	a-38:4	a-18:0/20:4	752·5599
24	**754·58**	**a-38:3**	**a-18:0/20:3**	**754·5756**
25	756·60	a-38:2	a-18:0/20:3	756·5912
26	758·62	a-38:1	a-18:0/20:2	758·6069
27	760·62	a-38:0	a-18:0/20:1	760·6225
G (5·0%)				
28	762·51	38:6	18:2/20:4	762·5079
29	764·52	38:5	18:1/20:4	764·5236
30	**766·54**	**38:4**	**18:0/20:4**	**766·5392**
31	768·56	38:3	18:1/20:2	768·5549
32	770·57	38:2	18:0/20:2	770·5705
33	772·59	38:1	18:0/20:1	772·5862
H (1·1%)				
34	**774·55**	**38:0 or a-40:7**	**e-18:1/22:6**	**774·5443**
35	776·57	a-40:6	a-18:1/22:5	776·5599
I (10·1%)				
36	788·54	40:7	18:2/22:5	788·5236
37	790·55	40:6	18:1/22:5	790·5392
38	**792·55**	**40:5**	**18:1/22:4**	**792·5549**
39	794·57	40:4	18:0/22:4	794·5705
40	796·59	40:3	18:1/22:2	796·5862
J (6·4%)				
41	820·59	42:5	18:0/24:5	820·5862
42	822·60	42:4	18:0/24:4	822·6018
43	**824·63**	**42:3**	**18:0/24:3**	**824·6175**
44	826·64	42:2	18:0/24:2	826·6331
45	828·67	42:1	18:0/24:1	828·6488

[a] All of the molecular species detected within a series are grouped by a letter are contained within the lowest and highest mass range and refers to the corresponding peaks in Fig. 5B. The percentages in parentheses correspond to the relative percentage based upon TIC. The peaks containing the most abundant PE species are in bold.
[b] As in Table S3.
[c] As in Table S1.
[d] As in Table S3.
[e] As in Table S1.

Table S5. Mass spectrometry analysis of PS molecular species in procyclic *T. brucei*

Peak[a]	*HR m/z*[b]	Lipid component[c]	Principal component[d]	*Theor m/z*[e]
A (1·0%)				
1	756·50	34:3	16:1/18:2	756·4821
2	758·50	34:2	16:0/18:2	758·4977
3	760·50	34:1	16:0/18:1	760·5134
4	762·54	34:0	16:0/18:0	762·5290
B (69·9%)				
5	768·50	a-36:4	a-16:0/20:4	768·5185
6	**770·54**	**e-36:2**	**e-18:1/18:2**	**770·5341**
7	**772·55**	**a-36:2**	**a-18:0/18:2**	**772·5498**
8	**774·58**	**a-36:1**	**a-18:0/18:1**	**774·5654**
9	776·59	a-36:0	a-18:0/18:0	776·5811
C (12·3%)				
10	784·52	36:3	18:1/18:2	784·5134
11	**786·54**	**36:2**	**18:0/18:2**	**786·5290**
12	**788·55**	**36:1**	**18:0/18:1**	**788·5447**
13	790·57	36:0	18:0/18:0	790·5603
D (12·4%)				
14	795·56	a-38:4	a-18:0/20:4	796·5498
15	**798·57**	**a-38:3**	**a-18:1/20:2**	**798·5654**
16	**800·60**	**a-38:2**	**a-18:0/20:2**	**800·5811**
17	**802·61**	**a-38:1**	**a-18:1/20:0**	**802·5967**
18	804·64	a-38:0	a-18:0/20:0	804·6123
E (1·2%)				
19	806·48	38:6	18:2/20:4	806·4977
20	808·52	38:5	18:1/20:4	808·5134
21	810·54	38:4	18:0/20:4	810·5290
22	812·57	38:3	18:1/20:2	812·5447
23	814·58	38:2	18:0/20:2	814·5603
24	816·58	38:1	18:1/20:0	816·5760
25	818·60	38:0	18:0/20:0	818·5916
F (3·1%)				
26	834·54	40:6	18:0/22:6	834·5290
27	836·57	40:5	18:1/22:4	836·5447
28	838·58	40:4	18:0/22:4	838·5603
29	840·60	40:3	18:1/22:2	840·5760
30	842·62	40:2	18:0/22:2	842·5916

[a] All of the molecular species detected within a series are grouped by a letter are contained within the lowest and highest mass range and refers to the corresponding peaks in Fig. 7A. The percentages in parentheses correspond to the relative percentage based upon TIC. The peaks containing the most abundant PS species are in bold.
[b] As in Table S3.
[c] As in Table S1.
[d] As in Table S3.
[e] As in Table S1.

Table S6. Mass spectrometry analysis of PE molecular species in bloodstream *T. brucei*

Peak[a]	*HR m/z*[b]	Lipid component[c]	Principal component[d]	*Theor m/z*[e]
A (1·1%)				
1	756·46	34:3	16:1/18:2	756·4821
2	758·47	34:2	16:0/18:2	758·4977
3	760·52	34:1	16:0/18:1	760·5134
4	762·53	34:0	16:0/18:0	762·5290
B (54·5%)				
5	768·53	a-36:4	a-16:0/20:4	768·5185
6	**770·54**	**e-36:2**	**e-18:1/18:2**	**770·5341**
7	**772·55**	**a-36:2**	**a-18:0/18:2**	**772·5498**
8	**774·57**	**a-36:1**	**a-18:0/18:1**	**774·5654**
9	776·60	a-36:0	a-18:0/18:0	776·5811
C (23·3%)				
10	784·53	36:3	18:1/18:2	784·5134
11	**786·55**	**36:2**	**18:0/18:2**	**786·5290**
12	**788·56**	**36:1**	**18:0/18:1**	**788·5447**
13	790·57	36:0	18:0/18:0	790·5603
D (6·0%)				
14	796·55	a-38:4	a-18:0/20:4	796·5498
15	798·57	a-38:3	a-18:1/20:2	798·5654
16	800·59	a-38:2	a-18:0/20:2	800·5811
17	802·62	a-38:1	a-18:1/20:0	802·5967
18	804·63	a-38:0	a-18:0/20:0	802·5967
E (2·4%)				
19	806·51	38:6	18:2/20:4	806·4977
20	808·52	38:5	18:1/20:4	808·5134
21	810·54	38:4	18:0/20:4	810·5290
22	812·54	38:3	18:1/20:2	812·5447
23	814·55	38:2	18:0/20:2	814·5603
24	816·57	38:1	18:1/20:0	816·5760
25	818·58	38:0	18:0/20:0	818·5916
F (12·0%)				
26	834·50	40:6	18:0/22:6	834·5290
27	**836·52**	**40:5**	**18:0/22:5**	**836·5447**
28	**838·53**	**40:4**	**18:0/22:4**	**838·5603**
29	840·55	40:3	18:1/22:2	840·5760
30	842·58	40:2	18:0/22:2	842·5916
G (0·4%)				
31	854·48	42:10	20:4/22:6	854·4977
32	856·50	42:9	20:5/22:4	856·5134
33	858·51	42:8	20:2/22:6	858·5290
H (0·2%)				
34	878·50	44:12	22:6/22:6	878·4977
35	880·52	44:11	20:6/24:5	880·5134
36	882·54	44:10	22:4/22:6	882·5290

[a] All of the molecular species detected within a series are grouped by a letter are contained within the lowest and highest mass range and refers to the corresponding peaks in Fig. 7B. The percentages in parentheses correspond to the relative percentage based upon TIC. The peaks containing the most abundant PS species are in bold.
[b] As in Table S3.
[c] As in Table S1.
[d] As in Table S3.
[e] As in Table S1.

Table S7. Mass spectrometry analysis of PI molecular species in procyclic *T. brucei*

Peak[a]	*m/z*	*HR m/z*[b]	Lipid component[c]	Principal component[d]	*Theor m/z*[e]
A (1·3%)	749	749·43	28:2	14:1/14:1	749·4246
1	750	750·48	IPC 32:1	Cer 32:1	750·4921
2	751	751·44	28:1	14:0/14:1	751·4403
3	752	752·50	IPC 32:0	Cer 32:0	752·5099
4	753	753·45	28:0	14:0/14:0	753·4559
5					
B (0·2%)					
6	761	761·46	e-30:3	e-16:2/14:1	761·4613
7	763	763·49	a-30:2	e-16:1/14:1	763·4767
8	765	765·50	a-30:1	a-16:0/14:1	765·4923
9	767	767·53	a-30:0	a-16:0/14:0	767·5080
C (2·9%)					
10	775	773·47	30:3	14:1/16:2	775·4403
11	777	777·49	30:2	16:1/14:1	777·4559
12	778	778·53	IPC 34:1	Cer 34:1	778·5234
13	779	779·51	30:1	16:1/14:0	779·4716
14	780	780·54	IPC 34:0	Cer 34:0	780·5412
15	781	781·52	30:0	16:0/14:0	781·4872
D (0·5%)					
16	789	789·48	e-32:3	e-16:2/16:1	789·4924
17	791	791·53	a-32:2	e-16:1/16:1	791·5080
18	793	793·55	a-32:1	a-16:0/16:1	793·5236
19	795	795·55	a-32:0	a-16:0/16:0	795·5393
E (1·0%)					
20	803	803·48	32:3	16:1/16:2	803·4716
21	805	8805·50	32:2	16:1/16:1	805·4872
22	806	806·55	IPC 36:1	Cer 36:1	806·5547
23	807	807·51	32:1	16:0/16:1	807·5029
24	808	808·57	IPC 36:0	Cer 36:0	808·5725
25	809	809·52	32:0	16:0/16:0	809·5185
F (0·4%)					
26	815	815·59	e-34:3	e-16:1/18:3	815·5080
27	817	817·54	e-34:2	e-16:1/18:2	817·5236
28	819	819·56	a-34:2	a-16:0/18:2	819·5393
29	821	821·57	a-34:1	a-16:0/18:1	821·5549
30	823	.823·59	a-34:0	a-16:0/18:0	823·5706
G (5·1%)					
31	829	829·52	34:4	14:0/20:4	829·4872
32	831	831·55	34:3	16:1/18:2	831·5029
33	832	832·58	IPC 38:1	Cer 38:1	832·5860
34	833	833·54	34:2	16:0/18:2	833·5185
35	834	834·64	IPC 38:0	Cer 38:0	.834·6038
36	835	835·56	34:1	16:0/18:1	835·5342
37	837	837·57	34:0	16:0/18:0	837·5498
H (5·8%)					
38	843	843·56	e-36:3, a-36:4	a-16:0/20:4	843·5393
39	845	845·55	e-36:2, a-36:3	e-18:1/18:2	845·5549
40	847	847·58	e-36:1, a-36:2	a-18:0/18:2	847·5706
41	849	849·57	e-36:0, a-36:1	a-18:0/18:1	849·5862
42	851	851·59	a-36:0	a-18:0/18:0	851·6019
I (56·6%)					
43	857	857·53	36:4	16:0/20:4	857·5185
44	859	859·52	36:3	18:1/18:2	859·5342
45	**861**	**861·54**	**36:2**	**18:0/18:2**	**861·5498**
46	**863**	**863·56**	**36:1**	**18:0/18:1**	**863·5655**
47	865	865·58	36:0	18:0/18:0	865·5811
J (1·2%)					
48	871	871·54	e-38:3 a-38:4	a-18:0/20:4	871·5706
49	873	873·56	e-38:2, a-38:3	e-18:1/20:2	873·5862
50	875	875·57	e-38:1, a-38:2	a-18:0/20:2	875·6019
51	877	877·58	e-38:0, a-38:1	e-18:1/20:0	877·6175
52	879	879·60	a-38:0	a-18:0/20:0	879·6332

Table S7. (*Cont.*)

Peak[a]	*m/z*	*HR m/z*[b]	Lipid component[c]	Principal component[d]	*Theor m/z*[e]
K (5·3%)					
53	879	879·54	38:7	16:1/22:6	879·5029
54	881	881·55	38:6	18:2/20:4	881·5185
55	883	883·57	38:5	18:1/20:4	883·5342
56	885	885·58	38:4	18:0/20:4	885·5498
57	887	887·59	38:3	18:1/20:2	887·5655
58	889	889·60	38:2	18:0/20:2	889·5811
59	891	891·63	38:1	18:0/20:1	891·5968
60	893	893·64	38:0	18:0/20:0	893·6124
L (0·5%)					
61	893	893·54	e-40:6	e-18:1/22:6	893·5549
62	895	895·54	e-40:5, a-40:6	a-18:0/22:6	895·5706
63	897	897·56	e-40:4, a-40:5	e-18:1/22:4	897·5862
64	899	899·59	e-40:3, a-40:4	a-18:0/22:4	899·6019
65	901	901·58	e-40:2, a-40:3	e-18:1/22:2	901·6175
66	903	903·61	a-40:2	a-18:0/22:2	903·6332
M (17·8%)					
67	903	903·49	40:9	20:4/20:5	903·5029
68	905	905·53	40:8	18:2/22:6	905·5185
69	907	907·55	40:7	20:2/22:5	907·5342
70	**909**	**909·56**	**40:6**	**18:0/22:6**	**909·5498**
71	**911**	**911·57**	**40:5**	**18:1/22:5**	**911·5655**
72	**913**	**915·58**	**40:4**	**18:0/22:4**	**913·5811**
73	**915**	**915·60**	**40:3**	**18:1/22:2**	**915·5968**
74	917	917·63	40:2	18:0/22:2	917·6124
75	919	919·66	40:1	18:1/22:0	919·6281
N (0·9%)					
76	927	929·54	42:11	20:5/22:6	927·5029
77	929	929·56	42:10	20:4/22:6	929·5185
78	931	931·56	42:9	20:5/22:4	931·5342
79	933	933·57	42:8	20:2/22:6	933·5498
80	935	935·57	42:7	20:5/22:2	935·5655
81	937	937·58	42:6	20:4/22:2	937·5811
82	939	939·63	42:5	18:1/24:4	939·5968
83	941	941·65	42:4	18:0/24:4	941·6124
O (0·7%)					
84	953	953·55	44:12	22:6/22:6	953·5185
85	955	955·56	44:11	20:6/24:5	955·5340
86	957	957·57	44:10	22:4/22:6	957·5498
87	959	959·58	44:9	22:4/22:5	959·5654
88	961	961·63	44:8	22:4/22:4	961·5811
89	963	963·64	44:7	20:2/24:5	963·5968

[a] All of the molecular species detected within a series are grouped by a letter are contained within the lowest and highest mass range and refers to the corresponding peaks in Fig. 8A. The percentages in parentheses correspond to the relative percentage based upon TIC. The peaks containing the most abundant PI species are in bold.
[b] As in Table S3.
[c] As in Table S1.
[d] As in Table S3.
[e] As in Table S1.

Table S8. Mass spectrometry analysis of PI molecular species in bloodstream *T. brucei*

Peak	m/z[a]	*HR* m/z[b]	Lipid[c]	Principal component[d]	*Theor* m/z[e]
G (0·8%)					
1	829	829·49	34:4	14:0/20:4	829·4872
2	831	831·54	34:3	16:1/18:2	831·5029
3	833	833·48	34:2	16:0/18:2	833·5185
4	835	835·53	34:1	16:0/18:1	835·5342
5	837	837·52	34:0	16:0/18:0	837·5498
H (0·8%)					
6	843	843·56	e-36:3, a-36:4	a-16:0/20:4	843·5393
7	845	845·53	e-36:2, a-36:3	e-18:1/18:2	845·5549
8	847	847·56	e-36:1, a-36:2	a-18:0/18:2	847·5706
9	849	849·51	e-36:0, a-36:1	a-18:0/18:1	849·5862
10	851	851·54	a-36:0	a-18:0/18:0	851·6019
I (26·8%)					
11	857	857·55	36:4	16:0/20:4	857·5185
12	859	859·54	36:3	18:1/18:2	859·5342
13	**861**	**861·52**	**36:2**	**18:0/18:2**	**861·5498**
14	**863**	**863·55**	**36:1**	**18:0/18:1**	**863·5655**
15	865	865·58	36:0	18:0/18:0	865·5811
J (0·5%)					
16	871	871·55	e-38:3 a-38:4	a-18:0/20:4	871·5706
17	873	873·55	e-38:2, a-38:3	e-18:1/20:2	873·5862
18	875	875·54	e-38:1, a-38:2	a-18:0/20:2	875·6019
19	877	877·54	e-38:0, a-38:1	e-18:1/20:0	877·6175
20	879	879·59	a-38:0	a-18:0/20:0	879·6332
K (4·2%)					
21	879	879·52	38:7	16:1/22:6	879·5029
22	881	881·54	38:6	18:2/20:4	881·5185
23	883	883·55	38:5	18:1/20:4	883·5342
24	885	885·55	38:4	18:0/20:4	885·5498
25	887	887·58	38:3	18:1/20:2	887·5655
26	889	889·56	38:2	18:0/20:2	889·5811
27	891	891·54	38:1	18:0/20:1	891·5968
28	893	893·59	38:0	18:0/20:0	893·6124
L (1·0%)					
29	893	893·54	e-40:6	e-18:1/22:6	893·5549
30	895	895·54	e-40:5, a-40:6	a-18:0/22:6	895·5706
31	897	897·56	e-40:4, a-40:5	e-18:1/22:4	897·5862
32	899	899·59	e-40:3, a-40:4	a-18:0/22:4	899·6019
33	901	901·58	e-40:2, a-40:3	e-18:1/22:2	901·6175
34	903	903·61	a-40:2	a-18:0/22:2	903·6332
M (63·1%)					
35	903	903·48	40:9	20:4/20:5	903·5029
36	905	905·50	40:8	18:2/22:6	905·5185
37	907	907·52	40:7	20:2/22:5	907·5342
38	**909**	**909·54**	**40:6**	**18:0/22:6**	**909·5498**
39	**911**	**911·54**	**40:5**	**18:1/22:5**	**911·5655**
40	**913**	**915·58**	**40:4**	**18:0/22:4**	**913·5811**
41	**915**	**915·59**	**40:3**	**18:1/22:2**	**915·5968**
42	917	917·60	40:2	18:0/22:2	917·6124
43	919	919·56	40:1	18:1/22:0	919·6281
N (1·3%)					
44	927	929·49	42:11	20:5/22:6	927·5029
45	929	929·54	42:10	20:4/22:6	929·5185
46	931	931·58	42:9	20:5/22:4	931·5342
47	933	933·53	42:8	20:2/22:6	933·5498
48	935	935·56	42:7	20:5/22:2	935·5655
49	937	937·59	42:6	20:4/22:2	937·5811
50	939	939·61	42:5	18:1/24:4	939·5968
51	941	941·67	42:4	18:0/24:4	941·6124
O (1·6%)					
52	953	953·52	44:12	22:6/22:6	953·5185
53	955	955·54	44:11	20:6/24:5	955·5340
54	957	957·56	44:10	22:4/22:6	957·5498

Table S8. (*Cont.*)

Peak	*m/z*[a]	*HR m/z*[b]	Lipid[c]	Principal component[d]	*Theor m/z*[e]
55	959	959·58	44:9	22:4/22:5	959·5654
56	961	961·61	44:8	22:4/22:4	961·5811
57	963	963·63	44:7	20:2/24:5	963·5968

[a] All of the molecular species detected within a series are grouped by a letter are contained within the lowest and highest mass range and refers to the corresponding peaks in Fig. 8B. The percentages in parentheses correspond to the relative percentage based upon TIC. The peaks containing the most abundant PI species are in bold.
[b] As in Table S3.
[c] As in Table S1.
[d] As in Table S3.
[e] As in Table S1.

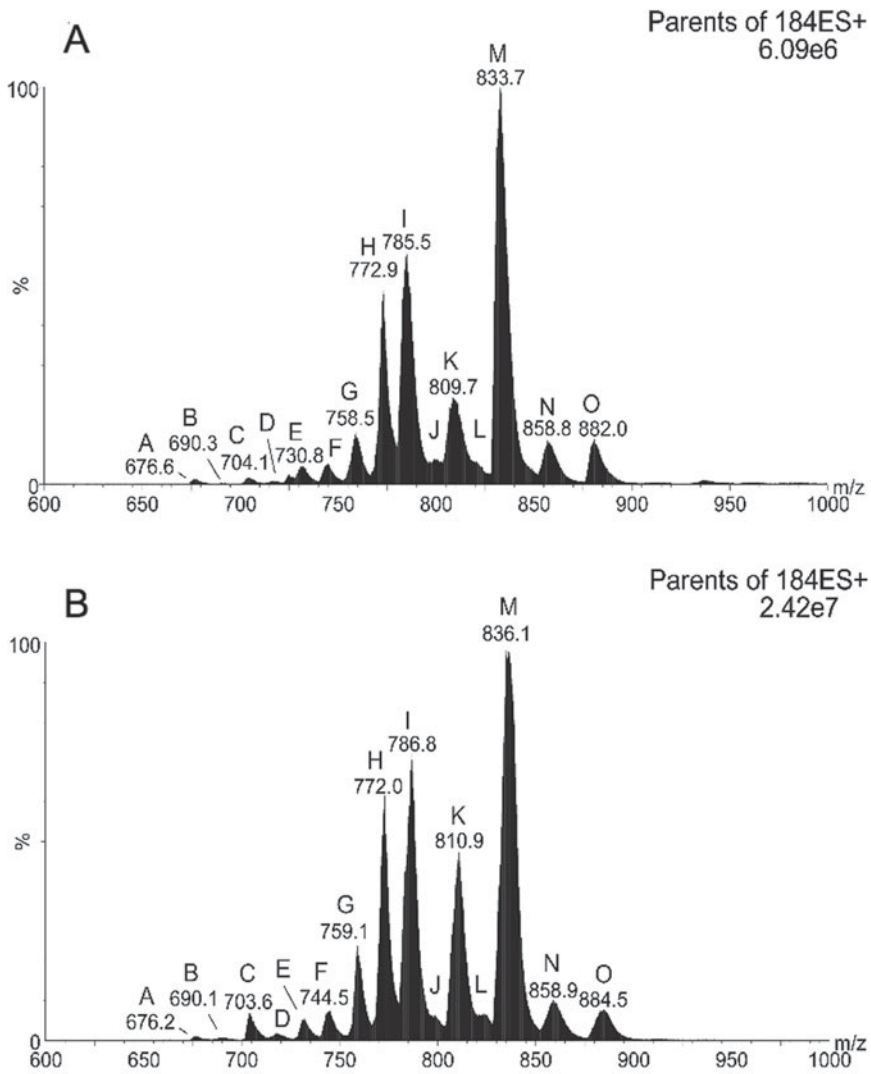

Fig. S1. ESI-MS-MS positive ion spectra of choline-containing PLs in *T. brucei*. Precursor ion scanning for *m/z* 184 specifically detected $[M+H]^+$ PC and SM ions from PCF (A) and BSF (B) trypanosome total lipid extracts. Peaks are plotted as their relative percent intensity (%) of the largest peak in the spectrum, and as a function of their mass/charge values (*m/z*). Peak assignments are based on MS-MS daughter ion spectra performed as stated in Material and Methods, and each peak series is annotated by a letter, which are annotated in Tables S1 and S2.

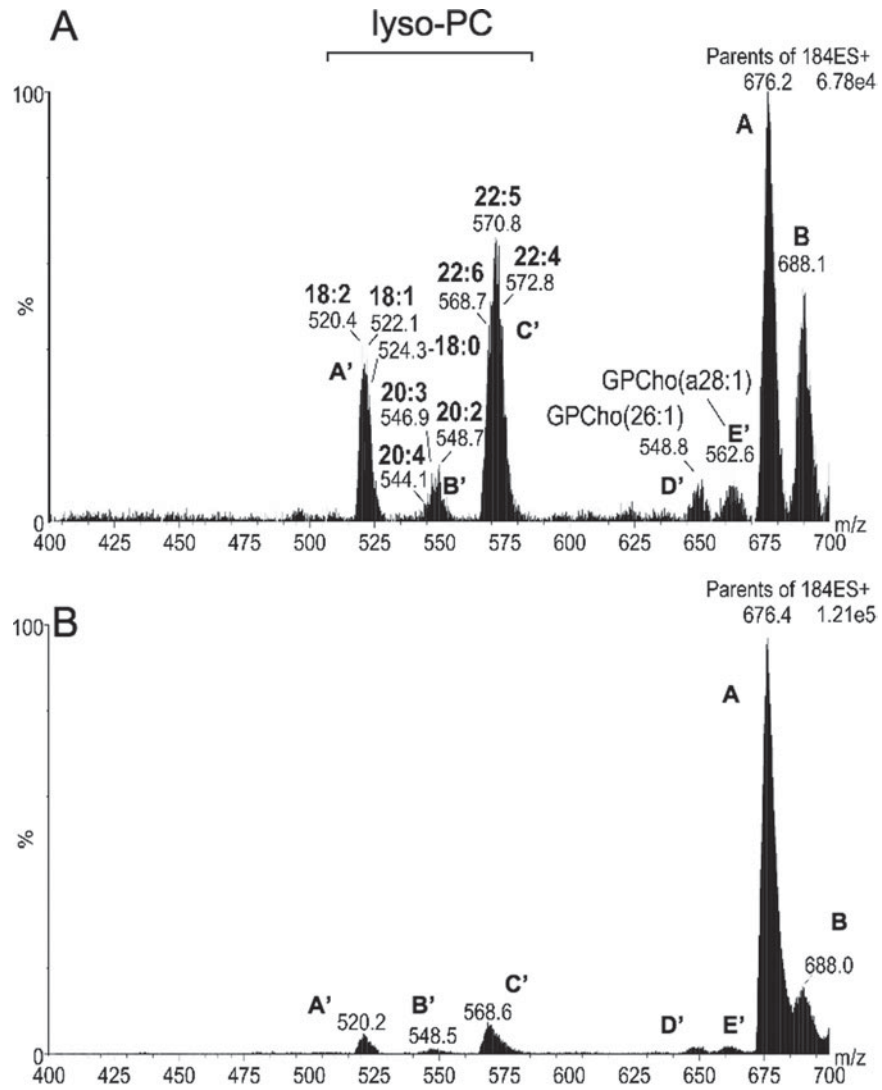

Fig. S2. ESI-MS-MS positive ion spectra of lyso-PC in *T. brucei*. Precursor ion scanning for m/z 184 specifically detected $[M+H]^+$ lyso-PC ions from BSF (A) and PCF (B) trypanosome total lipid extracts. Peaks are plotted as their relative percent intensity (%) of the largest peak in the spectrum, and as a function of their mass/charge values (m/z). The major lyso-PC signals were annotated based on their m/z value and MS-MS daughter ion spectra performed as stated in Material and Methods, and each peak series is annotated by a letter, which are annotated in Tables S1 and S2.

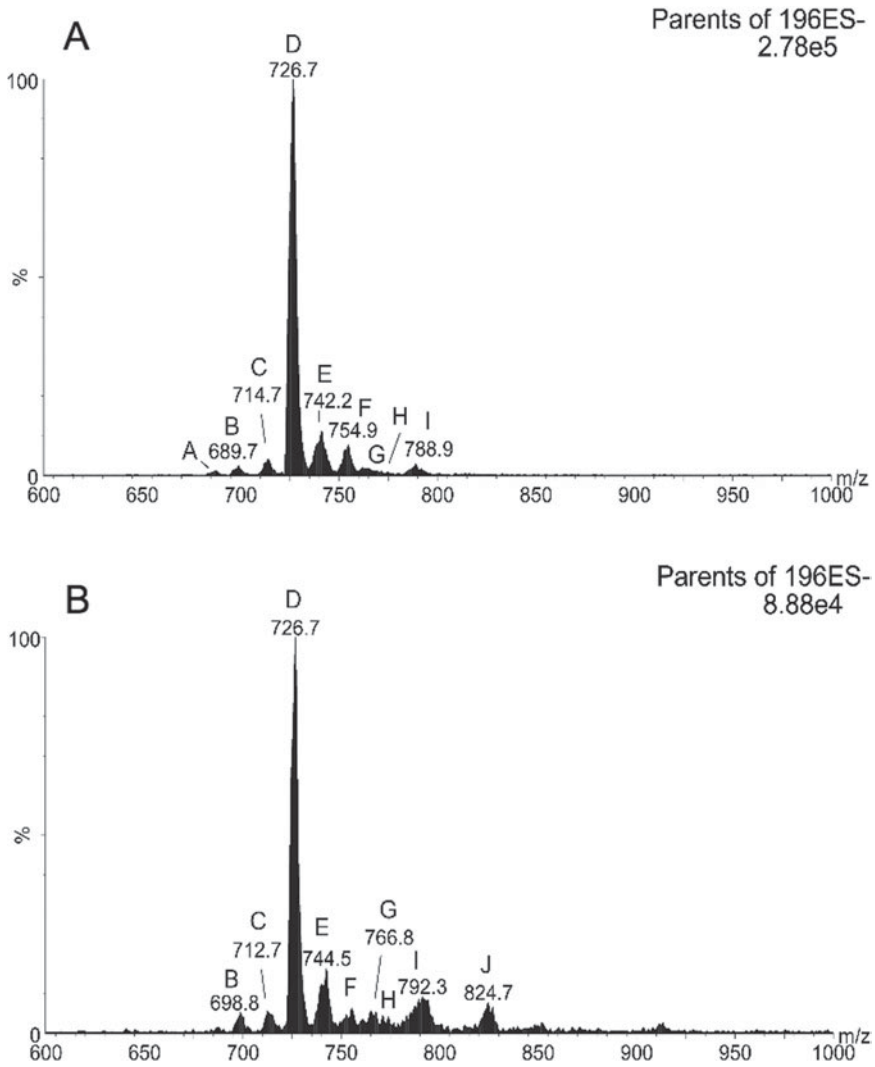

Fig. S3. ESI-MS-MS negative ion spectra of PE in *T. brucei*. Precursor ion scanning for *m/z* 196 specifically detected $[M-H]^-$ PE ions from PCF (A) and BSF (B) trypanosome total lipid extracts. Peaks are plotted as their relative percent intensity (%) of the largest peak in the spectrum, and as a function of their mass/charge values (*m/z*). Peak assignments are based on MS-MS daughter ion spectra performed as stated in the Material and Methods, and each peak series is annotated by a letter, which are annotated in Tables S3 and S4.

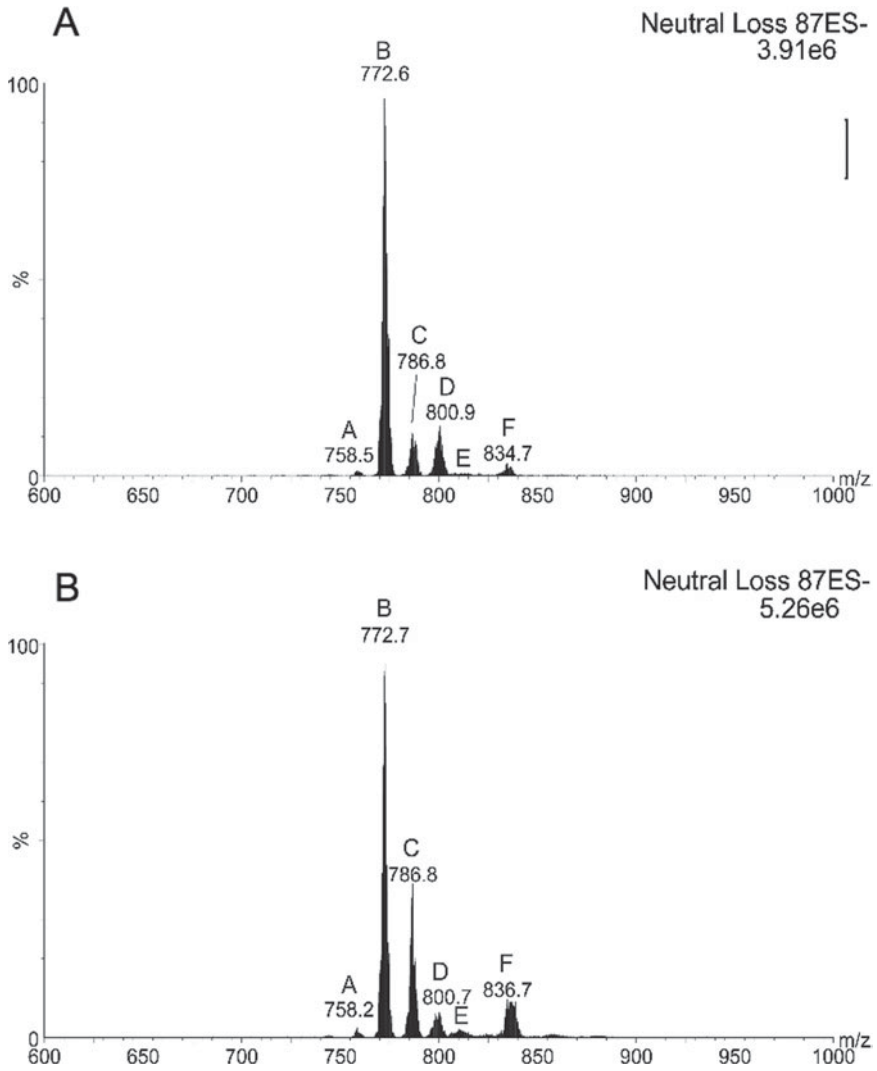

Fig. S4. ESI-MS-MS negative ion spectra of PS in *T. brucei*. Neutral loss scanning for *m/z* 87 specifically detected $[M-H]^-$ PS ions from PCF (A) and BSF (B) trypanosome total lipid extracts. Peaks are plotted as their relative percent intensity (%) of the largest peak in the spectrum, and as a function of their mass/charge values (*m/z*). Peak assignments are based on MS-MS daughter ion spectra performed as stated in Material and Methods, and each peak series is annotated by a letter, which are annotated in Tables S5 and S6.

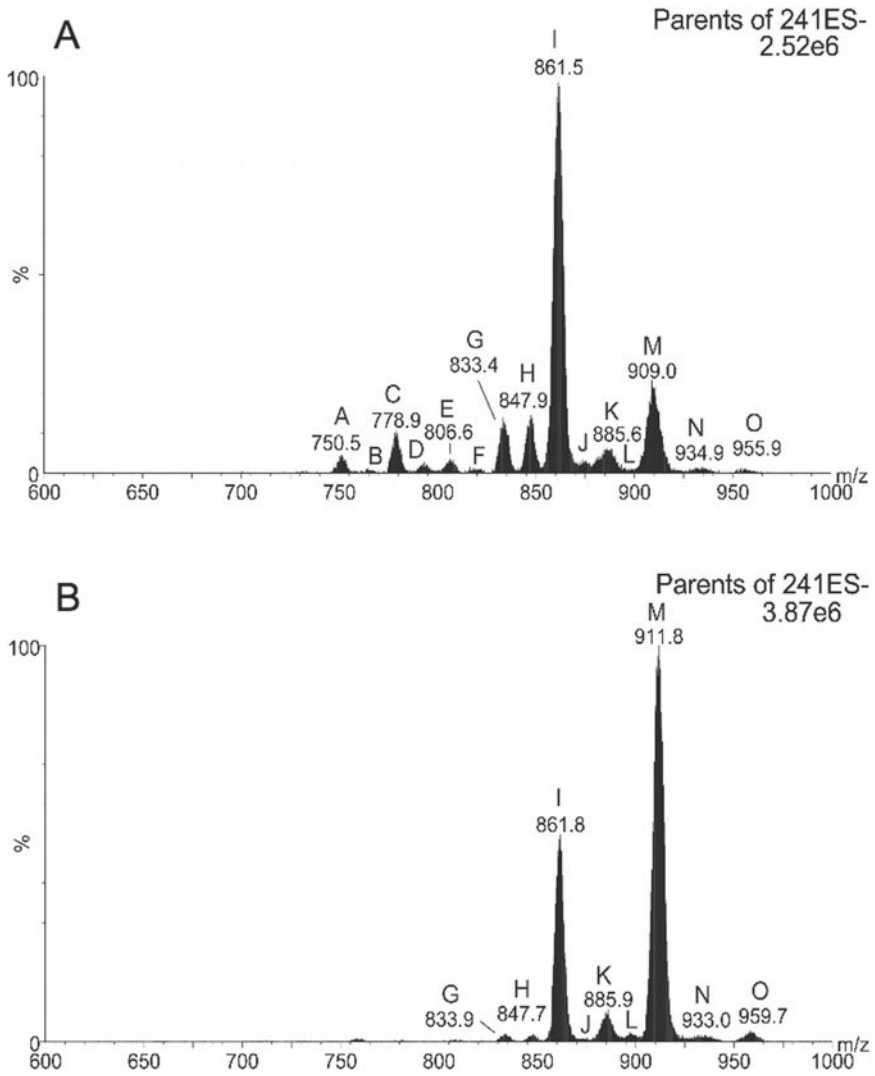

Fig. S5. ESI-MS-MS negative ion spectra of inositol-containing PLs in *T. brucei*. Precursor ion scanning for *m/z* 241 specifically detected $[M-H]^-$ PI and IPC ions from PCF (A) and BSF (B) trypanosome total lipid extracts. Peaks are plotted as their relative percent intensity (%) of the largest peak in the spectrum, and as a function of their mass/charge values (*m/z*). Peak assignments are based on MS-MS daughter ion spectra performed as stated in Material and Methods, and each peak series is annotated by a letter, which are annotated in Tables S7 and S8.

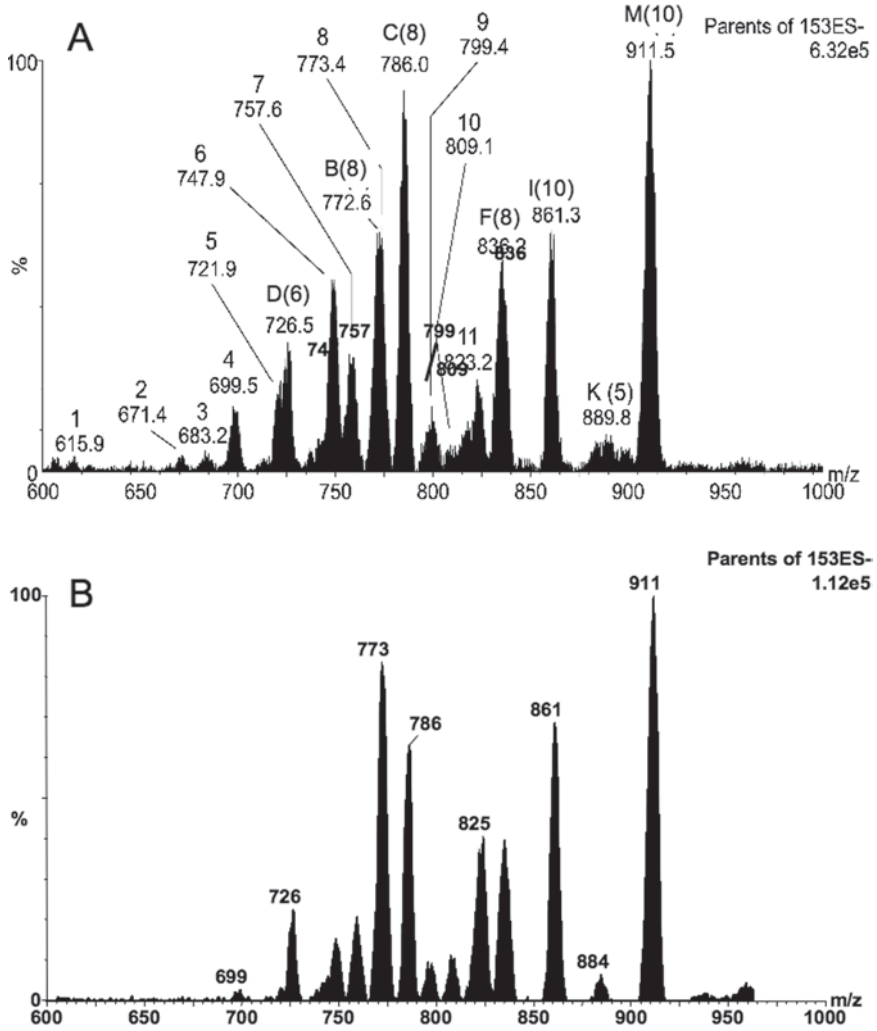

Fig. S6. ESI-MS-MS negative ion spectra revealing PA and PG molecular species in *T. brucei*. Precursor ion scanning for *m/z* 153 in negative ion mode with a collision offset energy of 50 V specifically detected $[M-H]^-$ ions from glycerophospholipids in a total lipid extract from PCF (A) and BSF (B) trypanosome total lipid extracts. (upper panel). Peaks are plotted as their relative percent intensity (%) of the largest peak in the spectrum, and as a function of their mass/charge values (*m/z*). Fatty acid assignments are based on the most intense fatty acid signals in the MS-MS daughter ion spectra (lower panel). Saturated fatty acids were assumed to be in the *sn*-1 position. Peaks labeled with a letter refer to the peak series that describes it in previous figures, to which the number in parentheses refers. Since each class of PL is detected with different optimal offset collision efficiencies, the PL class peaks in this spectrum do not accurately represent their true abundance in the cell relative to other PL classes. e = alkenyl; a = alkyl.